BIMODAL AGONISM: A NEW DESENSITIZATION IN A CYCLIC NUCLEOTIDE-GATED CHANNEL IS COORDINATED BY TWO ADJACENT BINDING DOMAINS

by

Kerry (Siu Cheong) Chan
B.Sc. Molecular Biology and Biochemistry, Simon Fraser University, 2006

THESIS SUBMITTED IN PARTIAL FULFILLMENT OF
THE REQUIREMENTS FOR THE DEGREE OF

MASTER OF SCIENCE

In the
Department
of
Molecular Biology and Biochemistry

SIMON FRASER UNIVERSITY

Fall 2008

APPROVAL

Name: **Kerry (Siu Cheong) Chan**

Degree: **Master of Science**

Title of Thesis: **Bimodal agonism: a new desensitization in a cyclic nucleotide-gated channel is coordinated by two adjacent binding domains**

Examining Committee:

Chair: **Dr. Bruce Brandhorst**
Professor, Department of Molecular Biology and Biochemistry

_____

Dr. Edgar C. Young
Senior Supervisor
Assistant Professor, Department of Molecular Biology and Biochemistry

_____

Dr. Rosemary B. Cornell
Supervisor
Professor, Department of Molecular Biology and Biochemistry

_____

Dr. Frederic F. Pio
Supervisor
Assistant Professor, Department of Molecular Biology and Biochemistry

_____

Dr. Peter C. Ruben
Internal Examiner
Professor and Director, School of Kinesiology

Date Defended/Approved: November 13th, 2008

ABSTRACT

Cyclic nucleotide-gated (CNG) channels are activated by direct binding of cyclic nucleotide (CN) to the binding domain (BD). How CN binding is coupled to channel opening remains unresolved. Bimodal agonism is found in the catfish olfactory CNGA2 subtype when cGMP is the agonist: initial cGMP binding events activate the channel while additional cGMP binding events deactivate the channel. The C-terminal region of the BD was previously shown to determine ligand selectivity and efficacy; therefore, this region from the normal (non-bimodal) BD was substituted into the bimodal BD. Excised patch-clamp measurements suggest that this region is not essential in bimodal agonism. We found a tandem tetramer with two adjacent bimodal pseudo-subunits can produce bimodal agonism whereas a tetramer with two diagonally opposing bimodal pseudo-subunits cannot. This implies that bimodal agonism does not require four bimodal BDs and the additional cGMP binding is coordinated by two adjacent bimodal BDs.

Keywords: CNG channel; desensitization; bimodal agonism; cGMP; cyclic nucleotide binding domain

DEDICATION

To my parents

ACKNOWLEDGEMENTS

I would like to express my gratitude to my senior supervisor Dr. Edgar Young for his excellent mentorship and guidance; this work would not have been possible without him. I would like to thank my supervisory committee, Dr. Rosemary Cornell and Dr. Frederic Pio for their helpful comments and suggestions throughout this project. I would also like to thank Dr. Peter Ruben for agreeing to act as my internal examiner, Dr. Bruce Brandhorst for chairing my defense and the MBB staff for their assistance. I have furthermore to thank the past and present members of the Young lab.

I would also like to thank my friends who have given me support throughout my graduate studies. Finally, I would like to thank the most important persons in my life, my parents and Cathy for their unconditional love, encouragement and support.

TABLE OF CONTENTS

LIST OF FIGURES

GLOSSARY

CNG	Cyclic nucleotide-gated channel
cGMP	Guanosine 3',5'-cyclic monophosphate
cAMP	Adenosine 3',5'-cyclic monophosphate
CNGA2	CNG channel subtype A2 cloned from the catfish olfactory epithelium
CNGA4	CNG channel subtype A4 cloned from the rat olfactory epithelium
TM	Transmembrane domain
BD	Cyclic nucleotide binding domain
I	Electric current
P_o	Channel open probability; the chance of observing an open channel at a given set of steady state condition
***Pro* action**	Cyclic nucleotide binding increase P_o
***Con* action**	Cyclic nucleotide binding decrease P_o
Critical residue	Amino acid residues unconserved between the CNGA2 and the CNGA4 BD essential for bimodal agonism
Conventional binding site	cGMP binding to this site increases P_o
Unconventional binding site	cGMP binding to this site decreases P_o
Xenopus	Genus of frog native to Africa
Tandem	One subunit covalently linked after another
Pseudo-subunit	A covalently linked subunit within the tandem oligomer
***Cis* configuration**	Like subunits arranged adjacent to each other in the tandem tetramers
***Trans* configuration**	Like subunits arranged diagonally opposite to each other in the tandem tetramers

CHAPTER 1: INTRODUCTION TO THE CYCLIC NUCLEOTIDE-GATED CHANNEL

1.1 Introduction to the cyclic nucleotide-gated channel

Ions carry a positive charge (cation) or a negative charge (anion). These charges render them unable to pass through the cell membrane's hydrophobic core. Ion channels are a class of membrane protein that allow ions to pass through the membrane's hydrophobic core. The direction of ion passage through ion channels depends on the permeant ion's concentration gradient as well as the electrical gradient across the membrane. Ion channels are classified based on: how they are gated (e.g. voltage-gated, ligand-gated, pressure-gated... etc) and the types of ions they transport (e.g. cation or anion). Ion channels are involved in many vital cellular processes; therefore, they are important therapeutic targets. Malfunctions in ion channels or channelopathies are the root of many diseases such as the long QT syndrome (abnormal heart repolarization associated with a potassium channel), cystic fibrosis (abnormal lung secretion associated with a chloride channel), and diabetes (mis-regulated insulin secretion associated with a potassium channel) (Kass, 2005). Ion channel studies could lead to new ways to cure ion channel related diseases.

The ion channel studied in this thesis is the Cyclic Nucleotide-Gated (CNG) channel. CNG channels are important in visual (Fesenko et al., 1985) and olfactory (Nakamura and Gold, 1987) signal transduction. The cation non-selective CNG channels are opened by direct binding of cyclic nucleotides such as guanosine 3',5'-cyclic monophosphate (cGMP) and adenosine 3',5'-cyclic monophosphate (cAMP). The CNG channel subunit contains conserved functional motifs. Four CNG channel subunits assemble into a functional channel. The CNG channel's structure, function and activation mechanism are reviewed in this chapter.

1.2 Subunit diversity in CNG channel

A functional CNG channel is assembled from four channel subunits (see "CNG channel is a tetramer", section 1.4). The main focus of my study is on the CNGA2 subunit cloned from the catfish olfactory neuron (Goulding et al., 1992) and the CNGA4 subunit cloned from the rat olfactory neuron (Bradley et al., 1994; Liman and Buck, 1994). There are six CNG channel genes identified and cloned from vertebrates through genome sequencing and molecular cloning to date. These subunits are further classified into two subfamilies, CNGA and CNGB, according to their primary amino acid sequence similarities (Kaupp and Seifert, 2002).

The CNGA subfamily contains CNGA1 first identified in retinal rod cells (Kaupp et al., 1989), CNGA2 first identified in olfactory sensory neurons (Dhallan et al., 1990; Ludwig et al., 1990), CNGA3 first identified in retinal cone cells (Bonigk et al., 1993; Weyand et al., 1994) and CNGA4 first identified in rat olfactory sensory neurons (Bradley et al., 1994; Liman and Buck, 1994).

The CNGB subfamily contains CNGB1 first identified in the rod photoreceptor (Korschen et al., 1995) and CNGB3 first identified in the cone photoreceptor (Gerstner et al., 2000).

CNGA1, A2 and A3 subunits can form functional homomers. They are considered to be the principal subunits. CNGA4, B1 and B3 cannot form functional homomers; these subunits co-assemble with the principal subunits to form functional channels (Zagotta and Siegelbaum, 1996; Kaupp and Seifert, 2002).

1.3 The CNG channel subunit contains functional modules

The CNG channel subunit is modular in architecture and contains several conserved functional modules. The CNG channel subunit topology is shown in Figure 1. Each subunit contains a cytosolic extreme N-terminus, followed by a transmembrane domain, followed by a cytosolic cyclic nucleotide binding region that consists of the C-linker region and the cyclic nucleotide binding domain. The

cytosolic extreme C-terminus follows the cyclic nucleotide binding domain. All known CNG channel subunits share the same architecture.

1.3.1 The transmembrane domain

The CNG channel's transmembrane domain (TM) contains six transmembrane helices (S1-S6) connected by loops (Henn et al., 1995). The amino acid sequence alignment between the CNG channel and the voltage-gated cation channels suggested that the TM is homologous among these channels and therefore they are structurally related (Jan and Jan, 1992). The transmembrane helices packing in the CNG channel is unknown, but due to the high sequence homology between the TM in the voltage-gated K^+ channel and CNG channel, the helices packing in the CNG TM is believed to closely resemble the TM from Kv1.2, a mammalian voltage-gated K^+ channel, which has a solved crystal structure (Long et al., 2005).

The fourth transmembrane helix (S4) in voltage-gated cation channels contain regularly spaced, positively charged residues (Jan and Jan, 1992). The S4 has been proposed to serve as the voltage sensor in the voltage-gated cation channels (Bezanilla, 2000). The TM in the CNG channel subunit also contains a homologous S4 transmembrane helix with regularly spaced, positively charged residues but CNG channel activation only has weak voltage dependence (Goulding et al., 1992).

1.3.2 The pore region

The CNG channel pore region is located in the TM. The pore sequence is homologous to the pore region in the voltage-gated cation channels (Jan and Jan, 1992). The re-entrant loop located between the transmembrane helix S5 and S6 lines the channel pore. CNG channels are non-selective cation channels. Both monovalent and divalent cations can permeate them (Zagotta and Siegelbaum, 1996). Divalent cations such as Ca^{2+} and Mg^{2+} permeate the channel at a slower rate than monovalent cations such as Na^+ and K^+. The flow of divalent cations slows down the flow of monovalent cations to decrease the

unitary channel conductance resulting in a phenomenon called the divalent cation block (Yau and Baylor, 1989; Zufall et al., 1994).

To minimize the effect of divalent cation block, divalent cation chelators were added to all buffers used in electrophysiology recordings in this study.

The divalent cation binding site responsible for divalent cation block in the CNG channel has been proposed to locate at the extracellular entryway of the CNG pore. In this model (Eismann et al., 1994; Root and MacKinnon, 1994), divalent cations binds to two identical, diagonally opposed binding sites formed from two conserved glutamate residues from two of the four channel subunits. Divalent cations binding slow down the flow of monovalent cations. Mutating the negatively charged glutamate residue to a neutral residue nearly abolishes divalent cation block in CNG channel suggesting that this conserved glutamate residues is responsible for divalent cation block.

The crystal structure of a bacterial voltage-gated Na^+ -K^+ conducting channel (NaK) with Na^+, K^+ and Ca^{2+} bound versions have been solved (Shi et al., 2006). The NaK channel is weakly selective between Na^+ and K^+ because the NaK selectivity filter, a structure in the ion channel that determines its permeant ion, is flexible; therefore, it can conform to different cations. Since both CNG and NaK channel have weak monovalent cation selectivity, the NaK channel pore is believed to closely resemble the CNG channel pore (Shi et al., 2006).

The Ca^{2+} bound NaK structure confirmed that the Ca^{2+} binding site is indeed located at the extracellular entryway of the pore. This structure also suggested that Ca^{2+}, instead of binding to the two identical, diagonally opposed binding sites proposed by Root and MacKinnon (Root and MacKinnon, 1994), binds to the glutamate's main chain carbonyl oxygen. Point mutation at this conserved glutamate residue may have changed the positions of the carbonyl oxygen to render them less flexible to bind divalent cation and therefore abolish the divalent cation block.

Goulding et al., compared single channel conductance in CNGA2 and CNGA1 and discovered that CNGA2 has a larger single channel conductance,

and exhibits less cation selectivity (Goulding et al., 1993 18). Organic cations with large ionic radii can pass through CNGA2 but not CNGA1; therefore the CNGA2 pore diameter is larger than the CNGA1 pore diameter (Goulding et al., 1993).

To test if the larger single channel conductance level in CNGA2 is due to its larger pore diameter, the pore region from CNGA2 was substituted into CNGA1 to create a chimera. The chimera and CNGA2 has the same single channel conductance level, thus the higher single channel conductance level in CNGA2 is due to its larger pore diameter (Goulding et al., 1993).

To ensure easily detectable channel current, all CNG channel subunits tested in this study contain the CNGA2 pore.

1.3.3 The N-S2 region

The N-S2 region spans from the middle of the extreme N-terminus to the end of the loop that connects the transmembrane helices S2 and S3 (Goulding et al., 1994) shown in Figure 5. The N-S2 region was identified to have a discrete function by regional substitution between CNGA1 and CNGA2. Substituting the entire N-S2 region from CNGA2 into CNGA1 increased the agonist efficiency in channel activation. Substituting either the N-terminus or the S2 region from CNGA2 into CNGA1 resulted in partial increase in channel activation (Goulding et al., 1994). Single channel recordings showed that unliganded openings occur more often in CNGA2 than in CNGA1. Unliganded openings were increased when the N-S2 region from the CNGA2 was substituted into the CNGA1; therefore, the N-S2 region from CNGA2 makes unliganded openings more energetically favourable (Tibbs et al., 1997).

All CNG channel subunits used in this study contain the N-S2 region from catfish CNGA2 to ensure robust channel activation.

1.3.4 The C-linker region

The C-linker region follows the end of the transmembrane helix S6 shown in Figure 5. It connects the cytosolic cyclic nucleotide binding domain to the TM. The C-linker region from CNGA1 contains a histidine residue that can bind Ni^{2+} to potentiate channel activation (increase cyclic nucleotide's potency). Ni^{2+} has no potentiating effects on CNGA2 because the histidine residue is substituted to a glutamine residue in CNGA2 (Gordon and Zagotta, 1995a). Ni^{2+} preferentially binds to the channel in the opened state (Gordon and Zagotta, 1995a). Two histidine residues from two adjacent subunits coordinate the Ni^{2+} binding sites (Gordon and Zagotta, 1995b 11).

All CNG channel subunits used in this study contain the C-linker region from CNGA1 so the option for Ni^{2+} potentiation is available when needed.

1.3.5 The cyclic nucleotide binding domain

The cyclic nucleotide binding domain (BD) follows the C-linker region. The BD is conserved in many proteins with diverse functions. The BD sequences from CNG channel, cAMP dependent protein kinase (PKA), cGMP dependent protein kinase (PKG), bacterial catabolite gene activator protein (CAP), and the hyperpolarization-activated cyclic nucleotide-modulated (HCN) channel are highly similar; therefore, they are believed to be homologous (Kaupp and Seifert, 2002). The BD crystal structures from CAP, PKA, Epac, HCN and a putative bacterial cyclic nucleotide gated ion channel have been solved (Weber and Steitz, 1987; Su et al., 1995; Zagotta et al., 2003; Clayton et al., 2004; Rehmann et al., 2008). The BD contains a beta roll that consists of eight anti-parallel beta strands folded into a jellyroll topology flanked by the A and B helices. The C helix connects to the B helix through a short loop (Weber and Steitz, 1987).

Residues important for cGMP and BD contact in the CNGA1 BD have been predicted from the CAP's BD crystal structure (Kumar and Weber, 1992). In particular, threonine 560 in the CNGA1 BD is predicted to hydrogen bond with the exocyclic phosphate oxygen from cGMP (Kumar and Weber, 1992). The

importance of this threonine residue in cyclic nucleotide selectivity in CNGA1 was tested with point mutation. When this threonine residue in CNGA1 is mutated to an alanine, the cGMP concentration required to reach half of the saturating current (EC50) increased by approximately 30 fold. Similarly, when this threonine residue is mutated to an alanine in the CNGA2 at the corresponding position, it increased the EC50 by approximately 40 fold (Altenhofen et al., 1991).

Recently, the mouse HCN2 BD structures were solved with cAMP or cGMP bound (Zagotta et al., 2003). The HCN BD crystal structures could provide structural insights to the CNG's BD because CNG and HCN channels are closely homologous in the BD (Craven and Zagotta, 2006). The HCN channels are hyperpolarization activated and modulated by cyclic nucleotide. Binding of cyclic nucleotides enhances channel activation (Craven and Zagotta, 2006). Both cAMP and cGMP can enhance HCN2 activation, but the EC50 for cAMP is 10 times lower than for cGMP (Zagotta et al., 2003).

The HCN2 BD crystal structure is particularly useful for this study because the BD structures were solved with cAMP or cGMP bound. Differences in the BD interactions with cGMP and cAMP can be observed by comparing the two structures. The HCN2 BD crystal structures showed that cAMP binds to the BD in the *anti* conformation while cGMP binds to the BD in the *syn* conformation (Zagotta et al., 2003). Surprisingly, the *syn* conformation of the cGMP bound to the HCN2 BD is consistent with the prediction made by Kumar and Weber from more than a decade ago (Kumar and Weber, 1992). This suggests that cGMP interactions with the BD are conserved in homologous BDs from different proteins.

Many attempts have been made to study how CNG channels discriminate between cAMP and cGMP. Goulding et al., proposed that the difference in cyclic nucleotide discrimination between CNGA2 and CNGA1 is localized in the C-helix (Goulding et al., 1994). Varnum et al., identified an aspartic acid residue located in the C-helix in the CNGA1 BD responsible for cyclic nucleotide discrimination. When this aspartic acid residue is substituted to a glutamine, CNGA1 exhibits

weak cyclic nucleotide selectivity similar to CNGA2, which has a glutamine at the corresponding position. When the aspartic acid residue is substituted to a methionine, CNGA1 exhibits reversed cyclic nucleotide selectivity and becomes highly selective for cAMP similar to CNGA4, which has a methionine at the corresponding position (Varnum et al., 1995). It is still unclear how cyclic nucleotide selectivity is achieved in different CNG channels.

1.4 CNG channel is a tetramer

The CNG channel is assembled from four channel subunits. This fact strongly influences the experimental design in this study. Several lines of evidence support the idea that CNG channel is a tetramer. CNG channel's primary amino acid sequence in the TM is highly homologous to the voltage-gated cation channels (Goulding et al., 1992; Jan and Jan, 1992). Several crystal structures of various K^+ channels from prokaryotes and eukaryote have been solved and showed that these K^+ channels are tetramers (Doyle et al., 1998; Zhou et al., 2001; Jiang et al., 2003; Long et al., 2005). Based on the homology between these channels, it is widely believed that the CNG channel, similar to the K^+ channels is also assembled from four channel subunits.

Liu et al., used a single channel conductance tagging approach to provide the first direct evidence that the CNG channel is indeed composed of four subunits (Liu et al., 1996). In the single conductance tagging approach, two types of CNG subunits with known single channel conductance levels were ligated to construct tandem dimers. Two types of tandem dimers were constructed: a dimer with two pseudo-subunits that have high single channel conductance (high-high dimer) and a dimer with two pseudo-subunits that have low single channel conductance (low-low dimer). The tandem dimers were co-expressed in *Xenopus* oocytes. If the CNG channel is a tetramer then two tandem dimers will assemble into a functional channel; therefore, only three types of single channel conductance levels (high, medium and low) will be observed. Two copies of the high-high dimer form a channel with high single channel conductance level, two copies of the low-low dimer form a channel with low single channel conductance

level and one copy of the high-high dimer co-assembles with one copy of the low-low dimer to form a channel with medium single channel conductance level. Single channel recordings were carried out and only three single channel conductance levels were observed in multiple recordings. This result strongly supports the idea that a functional CNG channel contains four subunits.

1.5 CNG channels are unique in the voltage-gated ion channel superfamily

The CNG channel belongs to the voltage-gated cation channel superfamily (Jan and Jan, 1992). CNG channels have several properties that make them unique in this superfamily. First, unlike other channels in this superfamily, CNG channels are gated by CN rather than voltage. Second, even though the CNG channel belongs to the voltage-gated cation channel superfamily, CNG channel activation is only weakly voltage dependent (Kaupp et al., 1989; Goulding et al., 1992). Finally, other channels in this superfamily are highly selective in the ion they transport but CNG channels are non-selective among monovalent cations.

1.6 CNG channel activation

CNG channels are gated by cyclic nucleotide such as guanosine 3',5'-cyclic monophosphate (cGMP) and adenosine 3',5'-cyclic monophosphate (cAMP). Cyclic nucleotide directly binds to the channel's cyclic nucleotide binding domain (BD) and activates the CNG channel (Kaupp and Seifert, 2002). Cyclic nucleotide binding can activate the CNG channel by stabilizing the open channel or by causing the channel's closed-to-open transition. Several studies have suggested that cyclic nucleotide binding is likely to stabilize the open channel rather than causing the channel to open.

The CNG channel can open in the absence of cyclic nucleotides (Picones and Korenbrot, 1995; Tibbs et al., 1997). The ability of CNG channel opening in the absence of cyclic nucleotide suggests that the CNG channel activation follows the cyclic allosteric mechanism (Monod et al., 1965). According to the

cyclic allosteric mechanism, the CNG channel can undergo closed-to-open transitions without any cyclic nucleotide bound. It also means that cyclic nucleotide binding stabilizes the channel's open state rather than causing the closed-to-open transition.

To explain how cyclic nucleotide binding stabilizes the open CNG channel, Goulding et al., proposed that the free energy difference due to the ligand binding reaction is coupled to the opening of the channel's gate (Goulding et al., 1994). Consider the CNG channel consisting of two coupled modules: the channel gate and the BD. The channel gate can exist in either the closed or the open state. The closed state has a lower free energy compared to the open state when there is no ligand bound; therefore, the channel gate's closed-to-open transition has a positive change in free energy and the channel gate stays in the closed state most of the time when the BD is not bound to cyclic nucleotide. The BD can exist in the ligand bound (activated) state or the ligand unbound (deactivated) state. The activated BD has a lower free energy compared to the deactivated BD; therefore, the ligand binding reaction has a negative change in free energy. Ligand can bind to the BD when the gate is in the open or in the closed state but the negative free energy change for binding is not the same for open channels and closed channels. Specifically, the free energy change for binding is much more negative when the gate is open than when the gate is closed. The negative change in free energy from the ligand binding reactions is coupled to the gate's closed-to-open transition to overcome the positive change in free energy associated with the gate's closed-to-open transition.

The CNG channel is assembled from four channel subunits (Liu et al., 1996 9) and each channel subunit has its own BD; therefore, each CNG channel has four BDs. Each ligand binding reaction contributes to the free energy coupling between the BD and the gate.

Several research groups have attempted to solve the exact contribution of each ligand binding step to channel activation. Liu et at. (Liu et al., 1998) incorporated either one, two or three BD mutants incapable of binding cyclic

nucleotide into a CNG channel. Channel open probabilities (P_o) of the CNG channels with different numbers of BD mutants were measured with single channel recording to find the relationship between the number of functional BDs and P_o. P_o is the chance of observing an open channel under a given experimental condition. Ruiz et al. (Ruiz and Karpen, 1999) used a different approach to find the relationship between P_o and the number of ligand bound. They tethered either one, two or three cGMP analogues to a CNG channel and measured their P_o using single channel recording. Biskup et al., used a fluorescent cGMP analogue to monitor ligand binding and P_o from normalized steady state current (Biskup et al., 2007).

The contribution of each ligand binding step to channel activation differed in all three studies, however, all three studies showed that P_o increases with increasing number of ligands bound. In addition, all three studies suggested that activation contributions from each ligand binding step are unequal; some ligand binding steps contribute more than other ligand binding steps.

1.6.1 Coupled-dimer activation model

The concept of CNG channel activation from two functional dimers were initially proposed by Liu et al., (Liu et al., 1998) when his research group attempted to solve the relationship between P_o and the number of ligand bound. Aside from finding the relationship between P_o and the number of bound ligand, Liu et al., found that the P_o values are different in a channel with two knocked-out BDs placed adjacent to each other (*cis*) than a channel with two knocked-out BDs placed diagonally opposite to each other (*trans*). This observation led Liu et al., to propose that CNG channels activate in a coupled-dimer fashion. In the coupled-dimer model, the four subunits in a CNG channel are arranged in two dimers. Within each dimer, the conformational changes in the two monomers are coupled to each other, so that the pair of monomers is a coupled-dimer. The channel will open only when both coupled-dimers in the channel are in the activated conformation.

HCN channels with two non-functional BD arranged in *cis* or *trans* arrangement had different activation behaviour; this suggests that the HCN channel also activates in a dimer-of-dimer fashion (Ulens and Siegelbaum, 2003). HCN and CNG channels belong to the voltage-gated ion channel superfamily. HCN channels are hyperpolarization activated and CN modulated. CN binding to the BD enhances channel opening. The enhancement of channel opening is measured by half maximal voltage ($V_{1/2}$) shift. $V_{1/2}$ is the voltage required to open half of the channel population. Ulens and Seigelbaum wanted to determine the energetic contribution of each CN binding to channel activation. They constructed a mutant HCN subunit with a non-functional BD and incorporated this mutant into tandem tetramers to constrain the number of functional BDs in the tandem tetramer. They found that the $V_{1/2}$ shifts are different when two functional BDs are adjacent to each other (*cis*) or diagonally opposite to each other (*trans*), suggesting that HCN channels also activates as dimer-of-dimer.

The mechanism for Ni^{2+} potentiation in CNGA1 also suggests a dimer-of-dimer symmetry. Gordon and Zagotta identified a histidine residue located in the C-linker region in CNGA1 that can bind Ni^{2+} to potentiate channel activation. Point mutation of this histidine residue abolishes Ni^{2+} potentiation. The wild type (wt) subunit and the histidine point mutant (mut) subunit were covalently joined to construct two types of hetero-tandem dimers: the wt-mut dimer and the mut-wt dimer. When the tandem dimers were expressed as homomers, the histidine residues in the wt pseudo-subunits are diagonally opposite to each other. This arrangement abolished Ni^{2+} potentiation. When the wt-mut dimer and the mut-wt dimer were co-expressed, two types of channels with two histidine residues from two adjacent wt pseudo-subunits (*cis*) and two histidine residues from two diagonally opposite wt pseudo subunits (*trans*) were formed. The *cis* channels restored Ni^{2+} potentiation; this suggested that the Ni^{2+} binding is coordinated by two histidine residues from two adjacent wt pseudo-subunits. This suggested that subunit interaction in Ni^{2+} potentiation has a two fold dimer-of-dimer symmetry. In

summary, three independent studies on CNG and HCN channels suggested that these channels are likely to activate in a dimer-of-dimer fashion.

1.7 Outstanding questions regarding CNG channels

There are still many unanswered questions regarding CNG channel activation. For instance, how much free energy does each cyclic nucleotide binding step contribute to the overall free energy in channel opening? What kind of conformational changes occur in the BD upon cyclic nucleotide binding? These questions are the fundamentals to understanding the CNG channel activation mechanism. Knowledge gained from studying CNG channel could have broader applications because some features in the CNG channel activation might be shared among the highly conserved voltage-gated ion channel superfamily. Knowledge gained from CNG studies could be extended to other important ion channels such as the HCN channel which is involved in heart pacemaking (Craven and Zagotta, 2006).

I am particularly interested in studying a new form of desensitization in a CNG channel called “Bimodal agonism”. Definition, bimodal agonism mechanism and specific hypotheses regarding bimodal agonism tested in this study are discussed in details in Chapter 2.

1.8 Introduction to the excised-patch clamp technique

The patch-clamp technique was invented by Neher and Sakmann in 1976 to study nerve impulses in frog muscle fibres (Neher and Sakmann, 1976). Since then, this powerful technique was modified to suit different needs in modern electrophysiological studies. The excised patch-clamp technique used in this study is a modified version of the original patch-clamp technique. A schematic representation of the excised patch-clamp set up is shown in Figure 2. In the excised patch clamp technique, a fine ended glass pipet filled with buffer solution is mounted onto a silver wire (electrode) which connects to an amplifier. Then a gigaohm seal is formed between the cell membrane and the glass pipet tip with

gentle suction. Once the gigaohm seal is achieved, the membrane is excised from the cell. The membrane potential of the excised membrane patch is “clamped” at a user specified voltage from the amplifier. The electrode clamps the membrane potential while changes in electric current are recorded. Once excised, the cytosolic side of the membrane is exposed to buffer that would mimic the cytosolic environment. The main advantage of the excised patch-clamp is the accessibility to the cytosolic side of the membrane. The excised patch-clamp allows buffers with or without cyclic nucleotide to access the CNG channel’s cytosolic BD to activate and deactivate the channels.

CHAPTER 2: INTRODUCTION TO BIMODAL AGONISM

2.1 Definition of bimodal agonism

Bimodal agonism is an agonist dependent, concentration dependent decrease in P_o observed in a CNG channel. The bimodal agonist has two distinct functional modes in depending on the number of bimodal agonist bound to the channel. Bimodal agonism is agonist dependent because it was only observed when cGMP was the agonist. It is also concentration dependent because at low concentration, initial cGMP binding increases P_o whereas additional cGMP binding at high concentration decreases P_o.

The dose-response curve of a bimodal channel shows that additional cGMP binding events decrease P_o. In bimodal agonism, there are two functionally discrete sets of BD-cGMP interactions in the bimodal (CNGA2) BD. These two sets of interactions operate at low and high cGMP concentrations, respectively. The first “conventional” set of BD-cGMP interactions exists at low concentrations. Binding of cGMP to the conventional binding site stabilizes the binding domain’s activated state to increase the P_o ("*pro*" action). The second unconventional set of BD-cGMP interactions has a much lower affinity; therefore, it exists at relatively higher concentration. Binding of cGMP to the unconventional binding site destabilizes the binding domain’s activated state to decrease the channel’s open probability ("*con*" action). A schematic illustration of the mechanism is shown in Figure 3.

The conventional and the unconventional binding sites could be structurally similar or distinct. In the scenario where the conventional and unconventional binding sites are structurally similar then at least one of these four binding sites (see “CNG channel is a tetramer”, section 1.4 for detail) serves as the unconventional binding site while the remaining binding sites serve as the conventional binding sites. In the alternative scenario where the conventional and

unconventional binding sites are structurally distinct, cGMP binding to the four CN binding sites is considered the conventional binding that increases P_o. Additional cGMP binding to somewhere else in the BD is considered the unconventional binding that decreases P_o. It holds true in both scenarios that additional binding of cGMP to the channel decreases P_o. My experiments were not designed to address whether the conventional and the unconventional binding sites are structurally similar or distinct; therefore, for simplicity of presenting the theory underlying our experiments, we will assume the conventional and unconventional binding sites to be structurally distinct. However, all conclusions of the thesis hold equally if the conventional and unconventional binding sites are structurally similar.

Bimodal agonism is extraordinary because the agonist binding has two roles: initial binding increases P_o while additional binding decreases P_o. Locating the unconventional binding sites will help us understand the mechanism of how cGMP binding to these unconventional binding sites decrease P_o. Finally, a thorough understanding of the mechanism underlying bimodal agonism could lead to designing CN analogues that can either strengthen or weaken the interactions with the unconventional binding site to allow precise control of the channel activity.

2.1.1 The bimodal channel current trace collected at high cGMP concentration illustrates the additional cGMP binding events

X-fA2 is a proven bimodal chimeric CNG channel from previous studies (Young et al., 2001). Steady state current from X-fA2 was measured at 10 mM and 30 mM of cGMP using the excised patch-clamp. The steady state current trace at these concentrations is shown in Figure 4. The steady state current level at 10 mM is less than the steady state current level at 3 mM. In the bimodal agonism mechanism, there are two sets of cGMP binding events in the bimodal channel. The conventional binding site is filled first because it has a higher cGMP affinity than the unconventional binding site. The conventional binding increases P_o (*pro* phase) and the unconventional binding decreases P_o (*con* phase). These

two sets of cGMP-BD interactions can be illustrated by comparing the shape of the bimodal channel current trace at 3mM and 10mM. The channel current trace collected with 3 mM cGMP shows no decrease in steady state current level. The channel current trace collected with 10 mM cGMP shows a decrease in steady state current level compared to the channel current trace collected with 3 mM cGMP. There is no decrease in steady state current level at 3 mM cGMP because 3 mM cGMP is not high enough for the unconventional interactions to occur. At higher cGMP concentrations such as 10 mM, the stable cGMP-unconventional binding sites interactions can occur.

The current trace collected with 10 mM cGMP showed a distinctive two spiked appearance. The first spike is associated with the cGMP wash in. During the wash in, cGMP concentration in the perfusion chamber increases and the P_o increases as cGMP binds to the conventional binding sites. The P_o reaches its peak when the conventional binding sites are saturated with cGMP, then as cGMP binds to the unconventional bimodal binding sites, the P_o decreases and reaches steady state. This increase then decrease in P_o is shown in the channel current trace as the first spike. The steady state current remains at the same level as long as the same concentration of cGMP is present. The second spike occurs during the cGMP washout. During wash out, cGMP concentration in the perfusion chamber decreases and the cGMP bound to the unconventional sites gets washed off first due to its lower cGMP affinity than the conventional interactions. The P_o increases back to the peak level as the unconventionally bound cGMP gets washed off to give rise to the second spike. The conventionally bound cGMP eventually gets washed off as cGMP concentration in the perfusion chamber decreases back to the baseline and the P_o decreases back to the basal level.

The peaks of the two spikes are comparable, suggesting that the decrease in steady state current is due to additional unconventional-cGMP binding. Binding and unbinding of the additional cGMP binding caused the current peaks. Thus, the appearance of the channel current trace at high cGMP concentration is consistent with the mechanism of bimodal agonism.

2.1.2 First observation of bimodal agonism in the catfish CNGA2 channel

Goulding et al., cloned the CNGA2 subunit from the catfish olfactory epithelium (Goulding et al., 1992). The cloned CNGA2 subunit was expressed as homomers in *Xenopus* oocytes and its dose-response behaviour was studied by measuring steady state P_o with cAMP and cGMP activation from a single channel. The cAMP dose-response curve showed that the P_o increases as cAMP concentration increases and it eventually reaches a plateau at high concentration. The cGMP dose-response curve showed that at low concentration, cGMP increases the channel open probability, the dose response curve peaks at 3mM and at higher concentration such as 10 mM the P_o decreases. This is the first record of bimodal agonism in CNG channel. Unfortunately, no follow up study on this phenomenon was done from this research group.

2.1.3 Bimodal agonism originates from the catfish CNGA2 BD

Young et al. (Young et al., 2001) constructed a series of chimeric CNG channels to study how ligand binding is coupled to channel opening. These chimeric CNG channels all carried identical amino acid sequences outside of the BD (see “Molecular subcloning of the X-chimera series”, section 3.2), but had different sequences in the BD. One of these chimeric channel had the BD from catfish olfactory CNGA2 while the other chimeric channel contained the rat olfactory CNGA4 BD. These chimeric channels were named X-fA2 and X-rA4 respectively. Single channel recording were done on X-fA2 and X-rA4 expressed as homomers, at various cAMP and cGMP concentrations. The cGMP and cAMP dose-response behaviour of X-rA4 showed no sign of bimodal agonism. In contrast, the cGMP dose-response curve of X-fA2 showed bimodal agonism. The dose-response curve of X-fA2 matched the cGMP dose-response curve of the cloned catfish CNGA2 channel measured by Goulding et al. This suggests that cGMP is a bimodal agonist and the BD from the CNGA2 is where bimodal agonism originates.

2.1.4 Known CNG channel activity modulation unlikely to cause bimodal agonism

Bimodal agonism is a new form of desensitization observed uniquely in the catfish CNGA2 BD. Reviewing previously observed desensitization in other CNG channels could provide us with new insights that might help us understand the mechanism underlying bimodal agonism better. Channel current decline can be caused by single channel conductance decrease or channel open probability decrease. In this section, several possible causes for current decline previously observed in CNG channel are contrasted with the current decline in bimodal agonism.

Root and MacKinnon identified a pair of independent proton transfer sites each formed by glutamate residues located at the extracellular opening of the CNG channel pore. Protonation of these glutamate residues decreases the rate of ion passage, thus decreases single channel conductance (Root and MacKinnon, 1994). I have considered the feasibility of explaining the current decline in bimodal agonism with this proton block model. All channel subunits tested in this study have identical amino acid sequence outside the BD. If proton block causes the current decline in bimodal channels then the same proton block effect should also be observed in X-rA4 which has the identical pore sequence. The lack of current decline in X-rA4 suggests that proton block is not the cause of current decline in bimodal agonism. All electrophysiology recordings in this study were held constant at -40 mV to drive inward current. The constant negative voltage should cause the proton block to remain at the blocking site. The recovery spike shown in the sample bimodal current trace (see Figure 4) suggests that proton block is unlikely to be the cause of current decline in bimodal agonism. Single channel recording on X-fA2 from previous studies showed that the single channel conductance remains the same at all cGMP concentrations (Young et al., 2001), suggesting that the current decline in bimodal agonism is due to a decrease in P_o rather than a decrease in single channel conductance. The arguments above suggest that the proton block model is inadequate to explain the current decline observed in bimodal agonism.

The glutamate residues responsible for proton block identified by Root and MacKinnon were mutated to neutral and small amino acid residues and a time-dependent current decline was observed in the mutants (Bucossi et al., 1996). Although all channels tested in this study have this glutamate unchanged, comparing the current decline in the mutants could provide insight to help us understand the current decline in bimodal agonism. The current decline due to the glutamate mutation is different than bimodal agonism in several aspects. The glutamate mutation causes a large conformational change at the pore as evidenced by the increased permeability to large organic cations and the long recovery time (at least 30 sec) required for the pore to recover from the desensitized state. The collapse of the pore is likely to be the cause of current decline in the glutamate mutant. In contrast, in bimodal agonism, the current is rapidly recovered from the desensitized state as shown in the second spike in the sample bimodal current trace. The recovery from desensitization in bimodal agonism is concentration dependent as evident by the association with cGMP wash out and therefore, the unbinding of cGMP. The difference in recovery time suggests that current decline in bimodal agonism is unlikely to be associated with a large conformational change such as the pore collapse in the glutamate mutants.

Desensitization has been reported when CNGA and CNGB subunits are co-expressed (Liman and Buck, 1994). CNGA and CNGB subunits are different in their ability to form a functional homomer. CNGA subunits can form functional homomers while CNGB subunits cannot. Liman and Buck found that when CNGA2 and CNGA4 are co-expressed, the channel current from this heteromeric channel declines at steady cAMP of 0.5 mM or higher. When the CNGA2 is expressed as homomers, the channel current showed no decline at steady cAMP at all concentrations (Liman and Buck, 1994). The origin of this desensitization could be from the BD or outside the BD. Shapiro and Zagotta constructed a chimera where the BD in the CNGA4 subunit was replaced with the CNGA2 BD. When this chimera was co-expressed with CNGA2, desensitization similar to the wildtype CNGA4 was observed at steady 1 mM cAMP (Shapiro and Zagotta,

2000). The chimera and the wildtype CNGA4 subunit had the same desensitization behaviour, suggesting that desensitization did not originate from the BD. In contrast, the current decline in bimodal agonism originated from the BD because X-fA2 and X-rA4 contain identical sequence outside of the BD but X-fA2 is bimodal and X-rA4 is not bimodal; therefore, the mechanism for current decline in bimodal agonism is different than the mechanism of current decline when alpha and beta subunits are co-expressed.

Calcium-calmodulin complexes directly bind to and inhibit CNG channels by increasing EC50 (Chen and Yau, 1994). The Ca^{2+}-calmodulin inhibition depends largely on the CNG tetramer composition because the Ca^{2+}-calmodulin binding sites were identified only in CNGA2, B1 and B3 (Trudeau and Zagotta, 2003). The Ca^{2+}-calmodulin inhibition cannot explain the decrease in current in bimodal agonism for several reasons. The divalent cation chelators present in the bath solution (see “Electrophysiology recording procedures”, section 3.5) should chelate Ca^{2+} to inhibit the Ca^{2+}-calmodulin inhibition. The lack of Ca^{2+} in the bath solution should favour the dissociation of Ca^{2+}-calmodulin complexes bound to the CNG channels resulting in increase in current rather than decrease in current. Time dependent run-up or run-down of channel current was tracked in all recordings by comparing steady state channel current at 3mM cGMP measured in various time after excision (see “Electrophysiology recording procedures”, section 3.5). The data collection did not commence until the run-up or run-down was over.

Molokanova et al., suggested that CNG channels expressed in oocytes are stably associated with protein tyrosine kinases (PTK) and protein tyrosine phosphatases (PTP) even after membrane excision. Phosphorylation and dephosphorylation decrease and increase channel activity, respectively (Molokanova et al., 1997). Several reasons suggest that this modulation is inadequate to explain the decrease in channel current in bimodal agonism. In this modulation, CNG channels are phosphorylated by PTK. The phosphate gradually gets dephosphorylated by PTP after excision resulting in an increase in channel current. Molokanova et al., showed that ATP, the substrate for PTK, can reverse

the increase in channel current. ATP is absent in the bath solution used in all of my experiments, yet the current fully recovers from its decline during bimodal agonism; therefore, phosphorylation by PTK cannot be the cause for the decrease in channel current in bimodal agonism. Furthermore, our methods of tracking run-up or run-down of channel current should minimize the effects of phosphorylation modulation in studying bimodal agonism; therefore, tyrosine phosphorylation and dephosphorylation cannot explain the mechanism underlying the current decline in bimodal agonism.

Several causes for current decline previously observed in CNG channels were compared with the current decline in bimodal agonism above. None of these causes can adequately explain the mechanism underlying the current decline in bimodal agonism, suggesting that bimodal agonism is a new form of desensitization in CNG channel.

2.2 Specific hypotheses tested in this study

Three specific hypotheses regarding the mechanism underlying bimodal agonism were tested in this study. First, I hypothesize that some amino acid residues in the CNGA2 BD are critical for producing bimodal agonism. Replacing any of these critical residues will result in the abolishment of bimodal agonism (see “Critical residue definition”, section 4.2). To test this hypothesis, regions from the CNGA4 BD were substituted into the CNGA2 BD to create BD chimeras. Bimodal activities of the BD chimeras were compared to identify regions in the CNGA2 BD that may contain critical residues (see “The C-terminal region of the CNGA2 BD does not contain critical residue”, section 4.5 for results).

Second, all observations of bimodal agonism were made when the bimodal channel subunit was expressed as homomers (Goulding et al., 1992; Young et al., 2001). I hypothesize that not all BDs in the CNG channel have to be bimodal in order to produce bimodal agonism (see “The BNNB tandem tetramer has bimodal activity at 30 mM cGMP”, section 5.6 for results).

Third, recent studies have suggested that the CNG channel and the closely homologous HCN channel activates in a coupled-dimer fashion (Liu et al., 1998; Ulens and Siegelbaum, 2003) (see “Coupled-dimer activation model”, section 1.6.1 for details). I hypothesize that the bimodal BD from different subunits in a CNG channel interact in a coupled-dimer fashion to produce bimodal agonism.

To test the hypotheses regarding intersubunit interactions in bimodal agonism and the requirement for four bimodal BDs, chimeric channel subunits carrying a bimodal or a normal BD were fused together to construct tandem tetramers (see “Tandem oligomers construction”, section 3.3). Tandem tetramers were designed to restrict the number and arrangement of channel subunits carrying bimodal and normal BDs in a CNG channel (see “The BNBN tandem tetramer showed no bimodal activity at 30 mM cGMP”, section 5.5 and “The BNNB tandem tetramer has bimodal activity at 30 mM cGMP”, section 5.6 for results).

CHAPTER 3: EXPERIMENTAL PROCEDURES

3.1 Computational analysis

3.1.1 Protein sequence alignments

Pairwise sequence alignments were done with the Blast 2 sequence algorithm (Tatusova and Madden, 1999) with default parameters. Multiple sequence alignments were done with the ClustalW2 algorithm (Larkin et al., 2007) with default parameters.

3.1.2 Comparative model building

The amino acid sequences of the cyclic nucleotide binding region (A' helix in the C-linker to the end of the C helix in the BD) from the catfish CNGA2 and rat CNGA4 were submitted to the SWISS-MODEL server, a fully automated protein structure homology-modeling server (Arnold et al., 2006). The homology models were predicted using the first approach mode using default settings. In brief, the SWISS-MODEL server first performs pairwise sequence comparison of the input sequence against all amino acid sequences in the Protein Data Bank to search for suitable templates with known 3D structures. The server then automatically chooses the top five sequences with highest sequence identity and uses them as templates. The template's structures were then averaged and weighted by their similarities to the input sequence to generate the model's core. Side chains were then added to the model based on the weighted positions of the corresponding residues in the templates. Superimpositions of the Cα atoms in the predicted models were done using DeepView, a model viewing and manipulating program (Guex and Peitsch, 1997).

3.2 Molecular subcloning of the X-chimera series

All CNG channel subunits were subcloned into the oocyte expression vector pGEM-HE (Liman et al., 1992). All CNG BDs tested in this study were subcloned into the X-chimera subunit shown in Figure 5. The X-chimera created in previous studies (Young et al., 2001) has invariant channel sequences outside the BD. All chimeras were constructed using standard PCR and restriction/ligation techniques (Sambrook, 2001). All genes for monomer subunits in this study were dideoxy sequenced in entirety, and cRNA was generated by *in vitro* transcription of the linearized plasmids (Ambion mMessage). The invariant sequences in the X-chimera consist of the bovine CNGA1 with its N-S2 region (CNGA1 N91-S240) replaced with the N-S2 region from the catfish CNGA2 (CNGA2 E89-R215) and the pore region (CNGA1 A344-A378) replaced with the pore region from catfish CNGA2 (S314-F348).

The BD sequence in X-fA2 was subcloned from catfish CNGA2 (CNGA2 L455-G584). The BD sequence in X-rA4 was subcloned from rat CNGA4 (CNGA4 L356-A485). The BD sequence in X-fr532 has L455-I533 from CNGA2 followed by K435-A485 from CNGA4. The BD sequence in X-fr496b has L455-K488 from CNGA2 followed by E390-I434 from CNGA4, followed by R534-P557 from CNGA2, followed by Q459-A485 from CNGA4. (see Figure 14 for BD sequences alignment)

3.3 Tandem oligomers construction

For construction of tandem dimers of the form M-N (where M and N are either X-rA4 or X-fr532 subunits), the gene sequences encoding individual M or N genes were fused by ligating compatible cohesive ends from non-identical restriction sites (Ulens and Siegelbaum, 2003), giving a ligation splice site that was resistant to restriction cleavage. In this case, the PspOMI cohesive end (found within gene M at its 3' end) was ligated to an EagI cohesive end (engineered into the plasmid bearing gene N, at a position 12 bp 5' of the start codon). In the resultant fusion protein, amino acids TDSTQD at the C-terminus of

subunit M were replaced with amino acids ST, followed by the initial methionine of subunit N. Pairs of tandem dimer genes were ligated in similar fashion to produce tandem tetramers (see Figure 6 for illustration). The presence of direct repeats in tandem dimers and tetramers precludes conclusive sequencing, so constructions were verified by restriction mapping (see section 5.2 for detailed description).

3.4 Testing tandem oligomers for correct pseudo-subunits order and composition

Tandem oligomers were constructed by fusing the bimodal subunit X-fr532 and the normal subunit X-rA4 together. The construction strategies for the tandem oligomers are shown in Figure 6. It is not possible to sequence the tandem oligomers to confirm pseudo-subunits composition because the bimodal and the normal subunits used in the tandem oligomer construction have identical sequences outside the BD. Also there are subunit duplications in the tandem tetramers. The sequencing primer can anneal to any one of the subunit duplicates making it impossible to confirm pseudo-subunits composition using sequencing. Therefore restriction digests were used to confirm pseudo-subunits order and composition in the tandem oligomers. A unique restriction cut site, EcoRV was strategically placed in the chimeric fr532 BD during the making of the X-fr532 subunit (see Figure 6).

To confirm the BN and the NB dimers' pseudo-subunit order and composition, the BN dimer was double digested with EcoRV and XbaI, while the NB dimer was double digested with EcoRV and NotI. Both XbaI and NotI are unique restriction cut sites located in the plasmid. XbaI and NotI were used to cut the BN dimer and the NB dimer, respectively, because the resulting restriction fragments sizes are easier to distinguish on gel electrophoresis. The double digestions yielded two fragments that matched the expected fragment sizes shown in Figure 7 and 8; therefore, the pseudo-subunit X-fr532 and X-rA4 were correctly fused together in the BN and the NB dimer constructs.

The tandem tetramer's pseudo-subunits order and compositions were confirmed with restriction digestion. Both of the BNBN and the BNNB tetramer were double digested with EcoRV and XbaI. XbaI is a unique restriction cut site located in the plasmid. The double digestions of the BNBN and the BNNB tetramers each yielded three fragments that matched the expected fragment sizes shown in Figure 9 and Figure 10, respectively, therefore the two Xfr532 pseudo-subunits and two X-rA4 pseudo-subunits were fused together in the correct order in the BNBN and the BNNB tetramer.

3.5 RNA transcription

Complementary RNA were *in vitro* transcribed from linearized plasmids carrying the channel constructs using mMESSAGE mMACHINE RNA transcription kit (Ambion). RNA transcripts were heat denatured and separated on gel electrophoresis to confirm the expected differences in molecular weight between monomer, dimer and tetramer genes (see section 5.2 for a detailed description). The RNA transcribed from the plasmids carrying the tandem oligomers were separated on denaturing gel shown in Figure 11. The monomer X-fr532 was loaded in lane 1 as a reference. The RNA gel picture showed that the monomer, dimers and tetramers have migrated different distances. The monomer migrated the longest distance because it has the smallest molecular weight. The dimers migrated less compared to the monomer because the dimers have higher molecular weight. The BN dimer and the NB dimer migrated the exact same distance. This suggests that both dimers have the same number of pseudo-subunits. The tetramers migrated the least distance compared to the monomer and the dimer because its molecular weight was the highest. The two tetramers migrated the exact same distance. This suggests that they have the same number of pseudo-subunits.

3.6 Electrophysiology recording procedures

All constructs were expressed in *Xenopus* oocytes by injection of cRNA and assayed in the excised patch-clamp configuration shown in Figure 2 (Hamill

et al., 1981) using previously reported procedures (Young et al., 2001). In brief: Oocytes were harvested from mature female *Xenopus laevis* frogs, defolliculated by collagenase (Sigma) and injected with 15-40 ng RNA; 1-7 days later, inside-out membrane patches were ex*ci*sed from oocytes, using heat-polished borosilicate glass micropipettes (0.5-5MΩ). Pipette and bath solutions both contained (in mM): 67 KCl, 30 NaCl, 10 HEPES, 10 EGTA, 1 EDTA, pH 7.2 with KOH. As needed, the sodium salts of cAMP (CalBiochem) and cGMP (Sigma) were included in the bath solution by iso-osmolar replacement of NaCl, and applied by gravity perfusion. Current data was acquired at room temperature (19-23°C) with an Axopatch 200B amplifier, filtered at 10kHz using the amplifier's low-pass Bessel filter, and recorded at 100 Hz by a Digidata 1322 and pClamp 9.0 software (Axon Instruments).

Patches were held at -40 mV and steady state currents in the presence of cyclic nucleotide were corrected by subtraction of leak currents in the absence of cyclic nucleotide. All data reported were collected after waiting a sufficient time for completion of spontaneous changes in channel activity (run-up or run-down), as shown by a difference of <5% among multiple measurements of current in 3 mM cGMP.

3.7 Statistical analysis

Unless otherwise noted, means are reported ± SD with N the sample size.

CHAPTER 4: THE N-TERMINAL REGION OF THE BIMODAL BINDING DOMAIN MAY CONTAIN CRITICAL RESIDUES

4.1 Critical residue definition

For the purpose of this study, a critical residue is defined as an amino acid at a specific position in the bimodal binding domain that is essential for the production of bimodal agonism. Bimodal agonism cannot occur without this specific amino acid. Critical residues are involved only in the unconventional set of BD-cGMP interactions if the conventional binding site and the unconventional binding site are structurally distinct. Alternatively, critical residues can be involved in the conventional interactions if the conventional binding sites and the unconventional binding sites are structurally similar. In the normal BD, only the conventional BD-cGMP interaction exists at all concentrations of cGMP and hence, there is no observed decrease in P_o at high concentration. We can contrast the critical residue with a "contributing" residue, which for the purpose of this study, is defined as an amino acid at a specific position in the bimodal binding domain that contributes to producing bimodal agonism but is inessential for it. For instance, if three residues are all part of an unconventional binding site, but two out of the three can form the site properly when the third is absent, the third residue would be contributing but not critical.

4.2 Bimodal agonism activity assessment

Bimodal agonism is a new form of desensitization. To assess the bimodal agonism activity in CNG channels, objective criteria have to be set to allow a systematic way to distinguish if a channel has bimodal activity or not. The chimeric channel X-fA2 shown in Figure 12 is a bimodal channel; it contains the CNGA2 BD cloned from catfish olfactory neuron. The chimeric channel X-rA4

shown in Figure 12 is a normal (non-bimodal) channel; it contains the CNGA4 BD cloned from rat olfactory neuron. The steady state P_o at various cGMP and cAMP concentrations for both X-fA2 and X-rA4 was measured using single channel recordings in previous studies (Young et al., 2001). In this thesis, X-fA2 and X-rA4 serve as the bimodal and normal control, respectively. A bimodal agonism activity assessment has been developed for this study. This assessment quantitatively assesses the decrease in P_o by comparing steady state channel current at 3mM with higher cGMP concentrations.

Macroscopic currents were measured in this study. In macroscopic current recording, electric current passing through multiple channels expressing in a membrane patch is recorded. The equation for macroscopic current (I) measured in this study is shown in Equation 1:

$$I = NP_o\gamma(V_m-E_{ion}) \qquad \text{Equation 1}$$

where N is the number of channels expressed in the membrane patch, P_o is the channel open probability, γ is the single channel conductance, V_m is the membrane potential held constant at -40 mV in all recordings and E_{ion} is the chemical potential of the permeant ion.

Previous studies have shown that the X-fA2 reaches maximum P_o at 3mM cGMP (Young et al., 2001); therefore, steady state channel current recorded at higher cGMP concentrations such as 10mM or 30mM (in the con phase) are divided by steady state channel current recorded at 3mM cGMP (peak) measured in the same patch to give a current ratio ($I_{XmMcGMP}/I_{3mMcGMP}$). The current ratio is related to P_o. For instance:

$$I_{10mMcGMP}/I_{3mMcGMP} = NP_{o10mMcGMP}\gamma(V_m-E_{ion})/\ NP_{o3mMcGMP}\gamma(V_m-E_{ion})$$

The terms N, γ and V_m are constant and E_{ion} is zero because the electrophysiology buffer on both side of the membrane contains identical permeant ion concentration, so the equation becomes

$$I_{10mMcGMP}/I_{3mMcGMP} = P_{o10mMcGMP}/P_{o3mMcGMP}$$

The current ratio was used to judge whether a channel is bimodal or not. The current ratio should equal unity if the P_o values are identical between the two cGMP concentrations compared. The current ratio should be less than one if the P_o value measured at the higher concentration is lower than the P_o value measured at 3 mM cGMP. The current ratio should be greater than one if the P_o value measured at the higher concentration is higher than the P_o value measured at 3 mM cGMP.

The recording apparatus is very sensitive to interferences such as electrical noise from the surroundings and it could potentially affect the data interpretation especially when the channel current is less than 100 pA. All channel current collected in this study ranges from 50 pA to 3 nA. The noise level varied from patch to patch. Typical noise fluctuation was around 10 pA. I have been cautious in reducing the electrical interference from the surroundings by building a faraday cage around the recording apparatus, shielding it from surrounding noise and carefully grounding all possible sources of noise inside the faraday cage. The current ratio of 0.95 was set to be the bimodal activity cut off to consider the noise issue when assessing bimodal activity. A channel is considered to be normal if the current ratio is higher than 0.95. In contrast, a channel is considered to be bimodal if the current ratio is less than 0.95. The published $P_{o10mMcGMP}/P_{o3mMcGMP}$ for X-fA2 is 0.88 (Young et al., 2001). This is considered to be bimodal in our bimodal activity assessment. There is no published $P_{o10mMcGMP}/P_{o3mMcGMP}$ for X-rA4 because the P_o saturates at 0.3mM cGMP; therefore, the $P_{o10mMcGMP}/P_{o3mMcGMP}$ was extrapolated to be 1 (Young et al., 2001). Macroscopic steady state current from the X-fA2 homomer and X-rA4 homomer activated by 3 and 10 mM cGMP was recorded in this study. A sample current trace for X-rA4 showing no steady state current decrease at high cGMP concentration (10 mM) is shown in Figure 13. The $I_{10mMcGMP}/I_{3mMcGMP}$ for X-fA2 and X-rA4 collected in this study are 0.61±0.05 (N=6) and 1.10±0.03 (N=8), respectively.

4.3 Putative cGMP-BD interactions in CNGA2 and A4 are predicted from the cGMP bound HCN2 crystal structure

The crystal structure of the BD with cGMP bound from a homologous ion channel HCN2 has been solved. This solved BD structure identified numerous amino acid residues making electrostatic, hydrogen bonding and non-polar interactions with the bound cGMP (Zagotta et al., 2003). I hypothesized that these cGMP-BD interactions are homologous between the HCN2, CNGA2 and A4 BDs, resulting in similar cGMP binding in HCN and CNG channels. Testing this hypothesis would allow me to identify putative cGMP binding sites in the CNGA2 and the CNGA4 BD to narrow down the number of possible critical residues. If the conventional and the unconventional cGMP binding pockets are structurally similar, then these cGMP-BD interactions could be both the conventional and the unconventional cGMP-BD interactions in the bimodal agonism mechanism. Alternatively, if the conventional and the unconventional cGMP binding pockets are structurally distinct, then these cGMP-BD interactions could be the proposed conventional cGMP-BD interactions in my main hypothesis.

To address this question, BD sequences from the beginning of the A helix to the end of the C helix from the mouse HCN2, catfish CNGA2 and rat CNGA4 are aligned. The BD sequences from HCN2 and CNGA2 are 35% identical and 56% similar. The BD sequences from HCN2 and CNGA4 are 33% identical and 58% similar. The BD sequences from CNGA2 and CNGA4 are 76% identical and 90% similar. The sequence identities and similarities values suggest that the HCN2, CNGA2 and CNGA4 BD are highly similar. The aligned BD sequences are shown in Figure 14. The HCN2 BD was compared to the CNGA2 and the CNGA4 BD because they belong to the voltage-gated ion channel family. The HCN2 crystal structure is solved with cGMP bound and the BD sequences in all three BD are highly similar as shown by the pairwise sequence alignments.

Ten amino acid residues in the HCN2 BD were identified to interact with the bound cGMP shown in Figure 14. Six of these cGMP contacting residues:

V564, L574, G581, E582, R591 and T592 identified in the HCN2 crystal structure are conserved in the CNGA2 and CNGA4 BD. Four other cGMP contacting residues: M572, C584, R632 and I636 identified in the HCN2 crystal structure were substituted to other residues in the CNGA2 and CNGA4 BD.

The side chain from M572 in the HCN2 BD lines the cGMP binding pocket with non-polar interaction; it is substituted to A504 in the CNGA2 BD and A405 in the CNGA4 BD. The small hydrophobic side chain from the corresponding Ala in the CNGA2 and the CNGA4 BD should have a similar non-polar interaction that lines the cGMP binding pocket.

The main chain nitrogen from C584 in the HCN2 BD forms a hydrogen bond with cGMP's cyclic phosphate; it is substituted to S516 in the CNGA2 BD and S417 in the CNGA4 BD. Since the hydrogen bond comes from the main chain nitrogen, the substitution in the CNGA2 and the CNGA4 BD should not affect this cGMP-BD interaction.

R632 in the HCN2 BD forms two interactions with cGMP: its side chain lines the cGMP binding pocket with non-polar interaction while its main chain carbonyl oxygen forms a long range hydrogen bond with cGMP's N1 nitrogen in the purine ring, mediated by a water molecule. R632 is substituted to I570 in the CNGA2 BD and I471 in the CNGA4 BD. This substitution should not affect its interactions with cGMP because the long range hydrogen bond is formed with the main chain carbonyl oxygen and the hydrophobic side chain from Ile can form similar non-polar interaction that lines the cGMP binding pocket.

The hydrophobic side chain from I636 in the HCN2 BD lines the cGMP binding pocket; it is substituted to Q574 in the CNGA2 BD and M475 in the CNGA4 BD. The non-polar interaction that lines the binding pocket should be similar in the CNGA2 BD because the Met side chain is capable of non-polar interaction as shown in M572 in the HCN2 BD. The side chain from Q574 in the CNGA4 BD should be able to retain this non-polar interaction because the C_{beta} and C_{delta} in the side chain could form non-polar interaction.

In summary, putative cGMP contacting residues in the CNGA2 and the CNGA4 BD are identified from the HCN2 BD crystal structure. The interactions between the putative contacting residues in the CNGA2 and the CNGA4 BD are homologous to the cGMP-BD interactions identified from the HCN2 BD crystal structure.

4.4 The putative cGMP-BD contacting residues conserved in both CNGA2 and A4 BDs are not essential in producing bimodal agonism

The sequence alignment between the HCN2, the CNGA2 and the CNGA4 BDs identified putative cGMP contacting residues in the CNGA2 and the CNGA4 BDs. The putative cGMP contacting residues are identical in CNGA2 and the CNGA4 BDs except Q574 in the CNGA2 BD and M457 in the CNGA4 BD. The residue substitution of M475 in CNGA2 for Q574 in CNGA4 cannot be the cause for the difference in bimodal activity between the CNGA2 and the CNGA4 BD. X-fr561, a BD chimera that contains this Q to M substitution was tested in previous studies (Young et al., 2001) and showed bimodal activity (see Figure 12). This suggests that this Q to M substitution did not cause the difference in bimodal agonism behaviour in CNGA2 and CNGA4.

P_o values of X-fA2 and X-rA4 activated with 3 and 10 mM cGMP were measured using single channel recordings in previous studies (Young et al., 2001). Macroscopic $I_{10mMcGMP}/I_{3mMcGMP}$ current ratios of X-fA2 and X-rA4 were collected and compared in this study (see Figure 12). The $I_{10mMcGMP}/I_{3mMcGMP}$ current ratio clearly showed that X-fA2 is a bimodal channel with a decrease in P_o at high cGMP concentrations while X-rA4 is not bimodal. Both A2 and A4 BDs contain identical cGMP-BD contacting residues yet they possess different bimodal activity. This suggests that these cGMP-BD contacting residues are different from the cGMP-BD contacting residues responsible for producing the decrease in P_o in bimodal agonism. In the mechanism, two sets of cGMP-BD interactions give rise to the *pro* and the *con* phase in bimodal agonism. The

cGMP-BD contacting residues conserved between A2 and A4 BDs could be participating in the *pro* phase in bimodal agonism.

4.5 The C-terminal region of the CNGA2 BD does not contain any critical residue

According to the definition of critical residue (see “Critical residue definition”, section 4.1) and if the critical residue is not conserved between the bimodal and normal BD then bimodal agonism can be abolished by substituting any part of the bimodal binding domain that encompasses any critical residue with the corresponding part from the normal binding domain.

To test this hypothesis, a series of chimeric binding domains was constructed by substituting parts of the normal CNGA4 BD to replace the corresponding parts in the bimodal CNGA2 BD. Each of the BD chimeras was then quantitatively assessed for bimodal agonism. If the substitution replaced a critical residue, the resultant channel should be normal. If the substitution replaced contributing residues, but no critical residues, the resultant channel should exhibit bimodal agonism, but perhaps with slightly different quantitative features compared to the original channel; for example, the cGMP concentration threshold for bimodal agonism might differ in the original and substituted channel. Finally, if the substitution did not replace any critical residues or contributing residues, the resultant channel should exhibit bimodal agonism identical in features with that of the original channel.

Previous work has tested a BD chimera, X-fr561 that contains no CNGA2 sequences after the B-helix (Young et al., 2001). X-fr561 is a bimodal channel; therefore, no critical residues are located in the C-helix. BD composition of X-fr561 is shown in Figure 12. The "loop-β8" region was identified to be important in agonist selectivity (Young and Krougliak, 2004). This region stretches from the loop following the P-helix to the eighth β-strand. That work also identified the B-helix as important in efficacy. I hypothesized that this region contains residues critical for bimodal agonism.

To test whether the residues in the β7-β8 and B-helix region of CNGA2 are critical for bimodal agonism, a new BD chimera, X-fr532, was constructed with CNGA2 sequence before and CNGA4 sequence after the β7. BD composition of X-fr532 is shown in Figure 12. Steady state channel current at different cyclic nucleotide concentrations was recorded using the excised patch-clamp. A sample current trace of X-fr532 activated with 3 and 10 mM cGMP is shown in Figure 15. Bimodal activity of X-fr532 was assessed using the $I_{10mMcGMP}/I_{3mMcGMP}$ current ratio. The current ratio and BD composition of X-fr532 is shown in Figure 12. The $I_{10mMcGMP}/I_{3mMcGMP}$ current ratio of X-fr532 is 0.72±0.09 (N=20) suggests that X-fr532 is a bimodal channel; therefore, the residues in the β7-β8 and B-helix region in the CNGA2 BD are not essential for bimodal agonism.

The BD chimera X-fr496b was constructed to test if there are any critical residues located in the region spanning β3 to the end of the C-helix. X-fr496b contains CNGA2 sequence from the A-helix to the end of β3, followed by CNGA4 sequence from the end of β3 to β7, followed by CNGA2 sequence from the end of β7 to the end of B-helix, followed by CNGA4 sequence from the end of B-helix to the end of the C-helix (see Figure 12). X-fr496b contains CNGA2 sequence from the end of β7 to the end of B-helix because results from X-fr532 showed that no critical residue is located within this region. A sample current trace of X-fr496b activated with 3 and 10 mM cGMP is shown in Figure 16. The $I_{10mMcGMP}/I_{3mMcGMP}$ ratio of X-fr496b is 0.78±0.15 (N=9) suggests that X-fr496b is bimodal; therefore, the residues unique to CNGA2 in the region from beta strand 3 to the carboxyl end of the BD is not essential for bimodal agonism.

In summary, if there exists a critical residue, it must be located at the amino end of the BD spanning the A helix to the beginning of beta strand 3. The BD chimera X-rf496 (CNGA4 BD sequence from the A helix to beta strand 3 and the rest of the BD sequence from CNGA2) would complete this test for critical residue, however, time was insufficient to test this construct thoroughly. Preliminary results from X-rf496 activated with 10 and 30 mM cGMP showed no

bimodal activity which suggests that critical residues are likely to be located in this region.

4.6 Critical residue predicted from the comparative models is a false hit

The high sequence similarities and identities between the catfish CNGA2, rat CNGA4 and mouse HCN2 BD sequences suggest that these three BDs are structurally highly similar. The crystal structure of the BD from the mouse HCN2 channel was solved (Zagotta et al., 2003). I hypothesized that residue substitutions between the CNGA2 and CNGA4 BD caused structural differences in the two BD, and as a result, their bimodal activities are different.

To test this hypothesis, the CNGA2 and CNGA4 BD sequences were submitted to the Swiss-model server (Arnold et al., 2006). The Swiss-model server predicted the three dimensional structures of the CNGA2 and CNGA4 BD using the HCN2 BD crystal structures as templates. The Cα atoms from the predicted CNGA2 and CNGA4 BD structures were superimposed with DeepView (Guex and Peitsch, 1997) to identify structurally different regions. The root mean square deviation (RMSD) of the Cα atoms measures structural deviation between two superimposed structures. The RMSD between the predicted BD structures of CNGA2 and CNGA4 is 0.4 Å suggests that the predicted BD structures of CNGA2 and CNGA4 are structurally similar.

A loop region in close proximity to the bound cGMP was identified to be structurally different between the two predicted structures. Within this loop region, a phenylalanine residue in the CNGA2 BD was identified to be important. The loop structure is sensitive to *in silica* mutation of the phenylalanine. When *in silica* mutated to a tyrosine residue, the loop shifts into a structure that resembles the loop in the CNGA4 BD shown in Figure 17. The predicted CNGA2 BD structure with its phenylalanine substituted to a tyrosine superimposed with the CNGA2 BD and CNGA4 BD with Cα RMSD of 0.32 Å and 0.25 Å, respectively. *In silica* substitution of this phenylalanine residue appears to change this loop

structure to resemble the loop in the CNGA4 BD; therefore, I hypothesized that this phenylalanine residue is a critical residue for bimodal agonism.

To test if this phenylalanine residue is a critical residue; the activation of X-fr496b expressed as homomers was tested with excised patch-clamp. X-fr496b has this phenylalanine residue substituted to a tyrosine residue (the asterisk marks the tyrosine substitution in Figure 12). The $I_{10mMcGMP}/I_{3mMcGMP}$ current ratio for X-fr496b is 0.78±0.15 (N=9). The current ratio suggests that X-fr496b is a bimodal channel; therefore, this phenylalanine predicted from the homology models is not a critical residue.

CHAPTER 5: TWO ADJACENT BIMODAL BINDING DOMAINS CAN PRODUCE BIMODAL AGONISM

Experimental results that will address my specific hypotheses regarding if all four BDs in a channel have to be bimodal in order to produce bimodal agonism and if the bimodal BDs interact in the coupled-dimer fashion to produce bimodal agonism are presented in this chapter.

5.1 The BD chimera X-fr532 was used as the bimodal pseudo-subunit in building the tandem oligomers.

The BD chimera X-fr532 is a bimodal channel. I hypothesized that the cGMP dose-response behaviour of X-fr532 is similar to the previously published bimodal channel X-fA2. Finding out if the cGMP dose-response behaviour of X-fr532 and X-fA2 are similar is important to downstream experiments because it narrows down the number of possible unconventional cGMP-BD contacts and tests the feasibility of using X-fr532 as the bimodal subunit in building the tandem oligomers for the intersubunit interactions experiments in later sections. If X-fr532 and X-fA2 exhibit different cGMP dose-response behaviour then the substituted BD region in X-fr532 might contain elements that contribute to bimodal agonism production; therefore, X-fr532 might not be suitable to use in building tandem oligomers.

To test this hypothesis, steady state current in X-fr532 was measured with 0.1 through 30 mM cGMP. Steady state currents at all cGMP concentrations were normalized to the steady state channel current at 3mM cGMP. The normalized steady state current were plotted against cyclic nucleotide concentration in a dose-response curve shown in Figure 18. The dose-response curve showed that steady state channel current or channel open probability increases with cGMP concentration up to 3mM and peaks at 3mM then decreases as cGMP concentration increases. X-fr532's cGMP dose-response

behaviour is similar to X-fA2; therefore, X-fr532 is a subunit with robust bimodal activity. X-fr532 was incorporated into the tandem oligomers as the bimodal pseudo-subunit.

5.2 The BN and NB tandem dimers expressed individually have no bimodal activity at 10mM of cGMP

CNG channels are assembled from four subunits. Each subunit contains one BD. All channel subunits tested so far have been expressed as homomers; therefore, all four BDs in the channel are identical. I hypothesized that not all BDs in the tetrameric channel have to be bimodal in order for bimodal agonism to occur. Finding the number of bimodal subunits required for bimodal agonism is important. It helps us to understand some basic aspect of bimodal agonism mechanism. For instance, the number of bimodal BDs required will tell us how the unconventional cGMP-BD interactions are coordinated.

To test this hypothesis, two tandem dimers: BN and NB were constructed. The tandem dimers are constructed by ligating two pseudo-subunits in tandem fashion. The pseudo-subunits are X-fr532, which has robust bimodal activity, and X-rA4, which has no bimodal activity. The BN tandem dimer contains the X-fr532 pseudo-subunit followed by the X-rA4 pseudo-subunit. The NB tandem dimer contains the X-rA4 pseudo-subunit followed by the X-fr532 pseudo-subunit.

The BN and NB dimers were expressed as homomers in oocytes. Two tandem dimers are expected to co-assemble into one functional channel with two bimodal and two normal BDs arranged in the *trans* configuration. A schematic representation of the BN dimer and NB dimer assembly as homomers are shown in Figure 19 and Figure 20, respectively. Steady state current was measured at 3 mM and 10 mM of cGMP. The $I_{10mMcGMP}/I_{3mMcGMP}$ current ratio for the BN dimer is 0.94±0.07 (N=5). The $I_{10mMcGMP}/I_{3mMcGMP}$ current ratio for the NB dimer is 0.96±0.03 (N=5). The $I_{10mMcGMP}/I_{3mMcGMP}$ current ratio suggested that a channel with two bimodal and two normal BDs arranged in the *trans* configuration has no bimodal activity. Alternatively, the removal of the two bimodal BDs increased the

cGMP concentration required to reach the *con* phase because there are simply less bimodal BDs to make the unconventional cGMP-BD interactions.

5.3 Co-expressing the BN and NB tandem dimers showed no bimodal activity at 10mM cGMP

When the two tandem dimers are co-expressed in equal amount, they are expected to co-assemble into four types of functional channels. Two types of these channels will have two bimodal and two normal BDs arranged in the *trans* configuration while the other two will have two bimodal and two normal BDs arranged in the *cis* configuration. A schematic representation of the dimers co-assembly is shown in Figure 21. Steady state current was measured at 3 mM and 10 mM cGMP. The $I_{10mMcGMP}/I_{3mMcGMP}$ current ratio for the co-expressed dimers are 0.99±0.05 (N=5); therefore, a channel with two bimodal and two normal BDs has no bimodal activity at 10mM cGMP. Alternatively, the removal of the two bimodal BDs could increase the cGMP concentration required to reach the *con* phase because there are simply less bimodal BDs to make the unconventional cGMP-BD interactions.

In theory, when the two tandem dimers are co-expressed in equal amount, there should be a one to one ratio of *cis* and *trans* channel in each membrane patch. In reality, the number of *cis* and *trans* channels depends largely on the population of channels captured in each membrane patch; therefore, the *cis* and *trans* channels contained in each membrane patch are expected to vary. For instance, if the *cis* channels are bimodal and the *trans* channel are normal but only a small number of the *cis* channels are captured in the membrane patch measured, then no decrease in the steady state current at high cGMP concentration will be observed. In addition, it may be the case in reality that one tandem dimer is expressed at higher amounts than the other. This could have a big impact on the current ratio that we rely on judging whether a channel is bimodal or not. In order to minimize this potential confounding effect, tandem tetramers are constructed and expressed individually to ensure that only one type of channel is present in each of the membrane patch measured.

5.4 The BNBN tandem tetramer showed no bimodal activity at 30 mM cGMP

Activation data from expressing each tandem dimers alone suggested that a channel with two bimodal and two normal BDs arranged diagonally opposite to each other (*trans*) has no bimodal activity at 10 mM cGMP. In contrast, when a bimodal subunit was expressed as a homomer, 10 mM cGMP was enough to decrease P_o. Two possibilities could lead to the lack of bimodal activity. The first possibility is that the removal of the two bimodal BDs increased the concentration of cGMP required to fill the unconventional cGMP binding site. The second possibility is the *trans* configuration simply cannot produce bimodal agonism at any cGMP concentration.

To distinguish these two possibilities, we constructed the BNBN tandem tetramer by ligating four pseudo-subunits in tandem fashion. The BNBN tetramer has X-fr532 pseudo-subunit followed by X-rA4 pseudo-subunit followed by another X-fr532 pseudo-subunit followed by another X-rA4 pseudo-subunit. A schematic representation of the BNBN tandem tetramer is shown is Figure 22. The advantage of testing BNBN tetramer is that each copy of the BNBN tetramer is expected to self-assemble into a single population of functional channel with its bimodal and normal BD fixed in the *trans* configuration. Steady state current of the BNBN tetramer was measured with 3, 10 and 30 mM of cGMP. The sample current trace of the BNBN tetramer shown in Figure 23 showed no decrease in steady state current level. The dose-response curve of the BNBN tetramer is shown in Figure 24. The dose-response curve reached a plateau above 3 mM cGMP suggests that the BNBN tetramer has no steady state current decline at high cGMP concentrations and thus it is not a bimodal channel. The average $I_{10mMcGMP}/I_{3mMcGMP}$ current ratio of the BNBN tetramer is 1.01±0.04 (N=13). This current ratio is similar to the current ratio measured in the individually expressed tandem dimers. The average $I_{30mMcGMP}/I_{3mMcGMP}$ current ratio of the BNBN tetramer is 1.05±0.11 (N=8). The current ratios suggest that the BNBN tetramer is not bimodal.

An interesting point to note is the standard deviation associated with the current ratio. The standard deviation of the average $I_{30mMcGMP}/I_{3mMcGMP}$ current ratio is 0.11. The standard deviation of the average $I_{10mMcGMP}/I_{3mMcGMP}$ current ratio is 0.04. The larger standard deviation associated with the average $I_{30mMcGMP}/I_{3mMcGMP}$ current ratio could suggest that some of the recordings might have bimodal activity. In fact, one recording did show bimodal activity at 30 mM cGMP; the $I_{30mMcGMP}/I_{3mMcGMP}$ current ratio for this particular recording is 0.87. Two possibilities could have given rise to this particular recording with a bimodal current ratio. The first possibility is that the channels expressing in this membrane patch are not the BNBN tetramer but rather a bimodal channel from anomalous assembly; therefore, the current ratio for this patch is different than other patches.

The second possibility is that the BNBN tetramer is bimodal but the decrease in P_o is masked by high P_o. The additional binding of cGMP to the unconventional site decreased P_o, but the introduction of the normal BDs increased P_o; as a result the decrease in P_o due to additional cGMP binding is cancelled by the increase in P_o due to the introduction of the normal BDs. This could explain why the majority of the recordings have a normal current ratio. The decrease in P_o was not masked in this patch; therefore, a bimodal current ratio was observed.

Cyclic-AMP cannot produce bimodal agonism; therefore, the P_o activated by cAMP can be used to deduce maximum P_o. If the BNBN tetramer has a high P_o, then same concentration of cAMP and cGMP would activate similar level of current. If the BNBN tetramer has a low P_o, then the current level activated by cAMP will be higher than cGMP at the same concentration. The cAMP and cGMP dose-response curves of the BNBN tetramer are shown in Figure 24. The cAMP and cGMP dose-response curves are similar; therefore, the BNBN tetramer has high P_o. This suggests that it is possible that the BNBN tetramer's bimodal activity is masked by the high P_o. BNBN tetramer's high P_o did not mask the bimodal activity in one patch suggesting that the channels expressing in this patch are unlikely to be BNBN tetramers.

In summary, the BNBN tetramer's $I_{30mMcGMP}/I_{3mMcGMP}$ current ratio is above 0.95; therefore, the BNBN tetramer is not bimodal (see "Bimodal agonism activity assessment", section 4.2).

5.5 The BNNB tandem tetramer showed bimodal activity at 30 mM cGMP

Activation data from the BNBN tetramer suggested that two bimodal BDs fixed in the *trans* configuration cannot produce bimodal agonism. I hypothesized that bimodal agonism can be produced with two bimodal BDs, but the BDs have to be arranged adjacent to each other.

To test the hypothesis, the BNNB tandem tetramer was constructed. The BNNB tetramer fixes two bimodal and two normal BDs adjacent to each other (*cis*). The BNNB tetramer has the same number of bimodal and normal BDs as the BNBN tetramer, but the BDs order is different. The BNNB tetramer contains a X-fr532 pseudo-subunit followed by a X-rA4 pseudo-subunit followed by another X-rA4 pseudo-subunit followed by another X-fr532 pseudo-subunit. A schematic representation of the BNNB tandem tetramer is shown is Figure 25. Similar to the BNBN tetramer, each copy of the BNNB tetramer is also expected to self-assemble into one functional channel with its two bimodal and two normal BDs fixed in the *cis* configuration.

Steady state current of the BNNB tetramer activated with 0.3 through 30 mM cGMP were measured. A sample current trace of the BNNB tetramer is shown in Figure 26. The dose-response curve of the BNBN tetramer is shown in Figure 27. The dose-response curve showed a decrease in current ratio at 30 mM cGMP suggesting that the BNNB tetramer's steady state current declines at high cGMP concentrations. The $I_{10mMcGMP}/I_{3mMcGMP}$ current ratio of the BNNB tandem tetramer is 0.99±0.03 (N=11). This suggests that the introduction of the two normal BDs increased the cGMP concentration requirement for reaching the *con* phase in bimodal agonism. The $I_{30mMcGMP}/I_{3mMcGMP}$ current ratio of the BNNB tandem tetramer is 0.87±0.05 (N=12); therefore, the BNNB tetramer is bimodal. This also suggests that two bimodal BDs in a tetramer are enough to produce

bimodal agonism. Comparing the $I_{30mMcGMP}$ /$I_{3mMcGMP}$ current ratios from the BNNB and BNBN tetramers suggested that the two bimodal BDs fixed in the *cis* configuration can produce bimodal agonism while fixing the two bimodal BDs in *trans* cannot.

CHAPTER 6: DISCUSSIONS AND CONCLUSIONS

6.1 Limitations to the tandem tetramer experiments

The activation data collected from the tandem oligomers were analyzed under the assumption that they were assembled into the expected channel tetramers. Although all tandem oligomer's subunit composition and order were confirmed with restriction digest, the possibility of anomalous assembly cannot be completely ruled out. However, some scenarios of anomalous assembly from diced tetramer can be ruled out. For instance, the scenario where the bimodal pseudo-subunits have broken off the BNNB tetramer and assemble into bimodal homomers is not feasible because the $I_{10mMcGMP}/I_{3mMcGMP}$ ratio is different than the $I_{10mMcGMP}/I_{3mMcGMP}$ ratio when X-fr532 was expressed as homomers. The scenario where the normal pseudo-subunits broken off the BNNB tetramer and assemble into normal homomers is also not feasible because the $I_{30mMcGMP}/I_{3mMcGMP}$ ratio clearly showed bimodal activity. Controls such as restriction digest were done to ensure the tetramer's integrity but one should keep an open mind on the possibility of anomalous tetramer assembly.

6.2 Tandem tetramer is a better system to study intersubunit interactions

In this study, two tandem tetramers were constructed to study intersubunit interactions in bimodal agonism. The tandem tetramers have two bimodal and two non-bimodal pseudo-subunits covalently joined such that the two bimodal subunits are adjacent or diagonally opposite of each other. The activation data from the tandem tetramer with two adjacent bimodal subunits suggest that two adjacent bimodal BDs are enough to produce bimodal agonism. This study is the first to utilize tandem tetramers to study intersubunit interactions in CNG channels. Before this study, intersubunit interactions (Gordon and Zagotta,

1995b, a; Liu et al., 1996; Liu et al., 1998) in CNG channels were studied through the co-expression of tandem heterodimers similar to the co-expression of the BN and NB tandem dimer in this study. The possible assemblies of co-expressed tandem heterodimers are shown in Figure 21. The shortcoming of co-expressing two different types of tandem dimers is that two populations of channels are expected. The balance between the two populations of channels depends on the expression level of each type of tandem dimers. Using tandem tetramers to study intersubunit interactions is advantageous over co-expressing tandem dimers because the tandem tetramer is expressed alone therefore only one population of channel is expected. This reduces the possible confounding effect associated with tandem dimer co-expression.

6.3 Bimodal agonism mechanism activates as coupled-dimer

Two tandem tetramers were tested in this study. The BNBN tetramer and the BNNB tetramer both contain two bimodal and two normal pseudo-subunits. The two tetramers differ from each other by the arrangement of their bimodal and normal pseudo-subunits. The BNBN (*trans*) tetramer has the two bimodal subunits diagonally opposite to each other while the BNNB (*cis*) tetramer has the two bimodal subunits adjacent to each other. Activation data suggest that the *trans* tetramer is not bimodal and the *cis* tetramer is bimodal. The difference in bimodal and normal pseudo-subunits arrangement must be contributing to the difference in bimodal behaviour.

My tandem tetramer experiment results are consistent with the coupled-dimer model (Liu et al., 1998). The observation when the channel has two functional BD, yet there are differences in P_o, is the foundation for the coupled-dimer model. Liu et al., has a large data set for one type BD arrangement but only one data point for the other type of BD arrangement. In contrast, my tandem tetramers have a more statistically significant data set for both types of tetramer. The results from my tandem tetramer experiment confirmed the coupled-dimer model by providing a larger, more statistically significant data set that showed

different behaviours when two subunits are constrained in different arrangements.

The difference in bimodal activity between the *cis* and the *trans* tetramers suggest that there is a preferred dimer assembly before the dimer of dimers assembly that makes up the functional channel. The four pseudo-subunits in the *cis* tetramer have two possible dimer assemblies shown in Figure 28A. In one possible assembly, the four pseudo-subunits can be assembled as two non-equivalent dimers: one dimer has two bimodal BDs and the other dimer has two non-bimodal BDs (horizontal split). In another possible assembly, the four pseudo-subunits can be assembled as two equivalent dimers each with one bimodal and one non-bimodal BD (vertical split). In contrast, the *trans* tetramer only has one possible assembly with two equivalent dimers each with one bimodal and one non-bimodal BD shown in Figure 28B (horizontal and vertical splits are equivalent). The dimer assemblies with one bimodal and one non-bimodal BD are equivalent in both of the *cis* and the *trans* tetramers. The non-equivalent dimer assembly is unique in the *cis* tetramer; therefore, it is likely to be the cause for the difference in bimodal activity among the two tetramers.

6.4 There are two unconventional cGMP binding sites in a bimodal homomer

The *cis* tetramer requires 30 mM cGMP to reach the *con* phase. In contrast, the bimodal subunit X-fr532 homomer only requires 10 mM cGMP to reach the *con* phase. This increase in cGMP concentration required to reach the *con* phase is likely due to the removal of two bimodal BDs in the *cis* tetramer. The difference in bimodal activity between the *cis* and the *trans* tetramer suggest that the unconventional cGMP binding is coordinated by two adjacent bimodal BDs. Together, these two results suggest that there are two unconventional cGMP binding sites each coordinated by two *cis* oriented bimodal BDs in a bimodal homomer channel. One of these two unconventional cGMP binding sites was removed in the *cis* tetramer; therefore, the cGMP concentration required to reach the *con* phase is increased.

6.5 Bimodal agonism does not require four bimodal binding domains

The BNNB tetramer is bimodal. This suggests that bimodal agonism does not require all four BDs in the channel to be bimodal. Two adjacent bimodal BD in a CNG channel is sufficient and necessary to produce bimodal agonism. Alternatively, the BBBN tandem tetramer with three bimodal BDs can also produce bimodal agonism because two of the three bimodal BDs in the tetramer are adjacent to each other. The BBBN tandem tetramer was not constructed because the conclusion of bimodal agonism does not require all four bimodal BDs hold true in both BNNB and BBBN tetramers.

6.6 Future direction

This study opened doors to new research areas that can help us to gain better understanding on the mechanism underlying bimodal agonism. Our BD substitution experiment suggested that there is no critical residue located within the region spanning the beta strand 3 to the carboxyl end of the BD. If a critical residue exists, the location for the critical residue would be between this A-helix to the beginning of beta strand 3. The existence of this possible critical residue can be tested with a construct with CNGA4 BD sequence from the A-helix to the beta strand 3 region and CNGA2 BD sequence for the beta strand 3 to the end of the BD. If this BD chimera is not bimodal then it would suggest that there are critical residues located in this region. Seven residues are unconserved between the CNGA2 and CNGA4 within this region. Each of these unconserved residues can be point mutated to pin point the critical residue.

Bimodal agonism has only been observed in the CNGA2 BD cloned from catfish olfactory neuron. We can test bimodal activities in other CNG BD by subcloning them into the X-chimera system to search for possible bimodal BD.

The N-S2 and pore region in the X-chimera system were subcloned from the catfish CNGA2. Activation data from the X-rA4 suggested that without the CNGA2 BD, these regions alone could not produce bimodal agonism. However,

the CNGA2 BD might be interacting with these regions to modulate bimodal activity. We can explore this possibility by substituting the N-S2 and pore region from other CNG channels into the X-chimera to test if the BD are interacting with these regions to modulate bimodal agonism.

6.7 Conclusion

Binding domain substitution experiments tested the presence of critical residues. Regions in the normal (non-bimodal) CNGA4 BD were substituted into the corresponding regions in the bimodal CNGA2 BD to form BD chimeras. Activation of the BD chimeras were tested and the results suggested that the there are no critical residues located in the C-terminal region of the bimodal BD. If critical residues exist, the N-terminal region of the bimodal BD is the most likely region that contains the critical residues (see Figure 29).

Tandem tetramers with covalently joined bimodal and normal pseudo-subunits were constructed and tested. Activation of a tandem tetramer with two bimodal and two normal pseudo-subunits arranged adjacent to each other showed bimodal agonism activity. This suggests that two bimodal subunits are enough to produce bimodal agonism. Furthermore, the tandem tetramer with two adjacent bimodal pseudo-subunits can produce bimodal agonism while a tandem tetramer with two diagonally opposing bimodal pseudo-subunits cannot. This suggests that the arrangement of bimodal subunits affects bimodal agonism and the additional cGMP binding events that cause deactivation are coordinated by two adjacent bimodal subunits. This could narrow down our search for the additional cGMP binding pocket to the interface between two adjacent bimodal BD (see Figure 29).

FIGURES

Figure 1 CNG channel topology.

All known types of CNG channel subunits share the same topology. The extreme amino terminus is located on the cytosolic side of the membrane. The transmembrane domain (TM) follows the extreme amino terminus. The TM contains six transmembrane helices S1 - S6. The S4 helix contains regularly spaced positively charged residues. The extended loop located between the transmembrane helices S5 and S6 lines the channel pore. The C-linker region connects the TM to the cytosolic cyclic nucleotide binding domain (BD). The C-linker region and the BD make up the cyclic nucleotide binding region. The extreme carboxyl terminus follows the BD on the cytosolic side of the membrane.

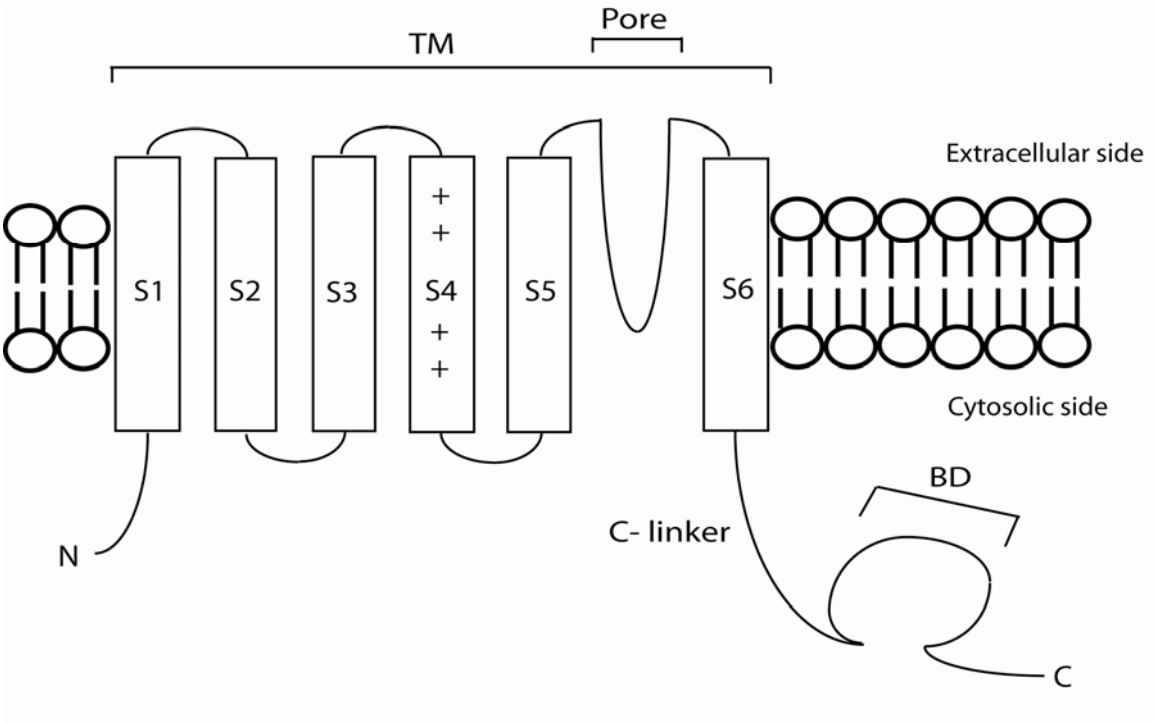

Figure 2 The excised patch-clamp apparatus.

The excised patch-clamp set up is shown in A. Solutions are perfused to the excised membrane patch through a gravity flow perfusion system controlled by a manual valve. The electrode is filled with bath solution. The electrode is connected to the amplifier which held the membrane potential constant. The reference wire completes the electric circuit. Close up view of the electrode's aperture is shown in B. The orange surface represents the membrane patch. The black boxes represent ion channels captured in the membrane patch. The cytosolic side of the membrane is exposed to bath solution in excised patch-clamp.

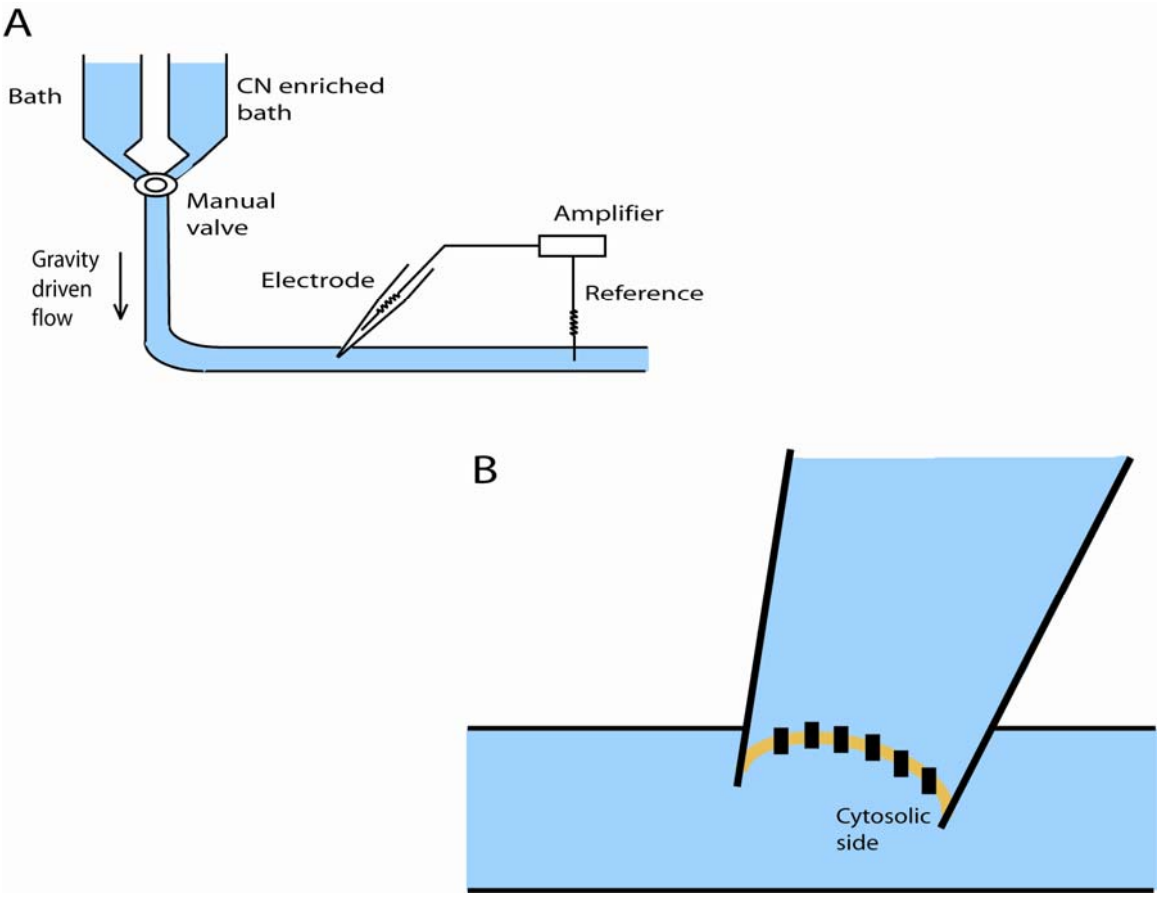

Figure 3 Bimodal agonism mechanism.

Normal agonism and bimodal agonism are compared in this hypothetical dose-response curve. Dose-response curves for normal agonism and bimodal agonism are shown in blue and red, respectively. The square represents a closed channel and circle represents an open channel. The half squares and half circles in bimodal agonism represent the unconventional cGMP binding sites proposed in my hypothesis. The thickness of the arrows indicate which side is the equilibrium favoured.

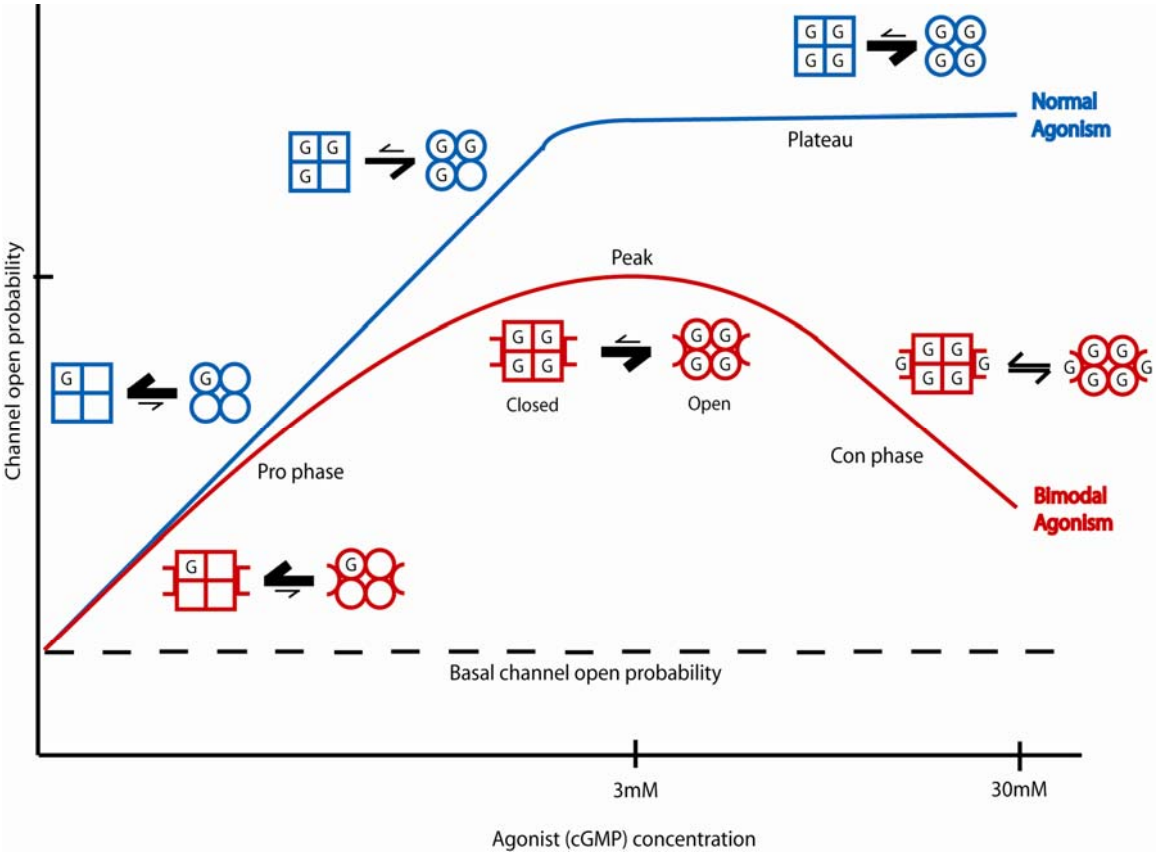

Figure 4 Sample current trace from the bimodal channel X-fA2.

Messenger RNA *in vitro* transcribed from the plasmid containing X-fA2 was injected into *Xenopus* oocytes to express X-rA2 as homomers. Activities from X-fA2 were recorded using the excised patch-clamp technique. The patch voltage was held constant at -40 mV. Cyclic-GMP enriched bath solutions were perfused to the membrane patch with a gravity flow perfusion system to activate the channels. The solid line represents the presence of cGMP and the dotted line represents the cGMP wash out. The dash line marks the zero current level.

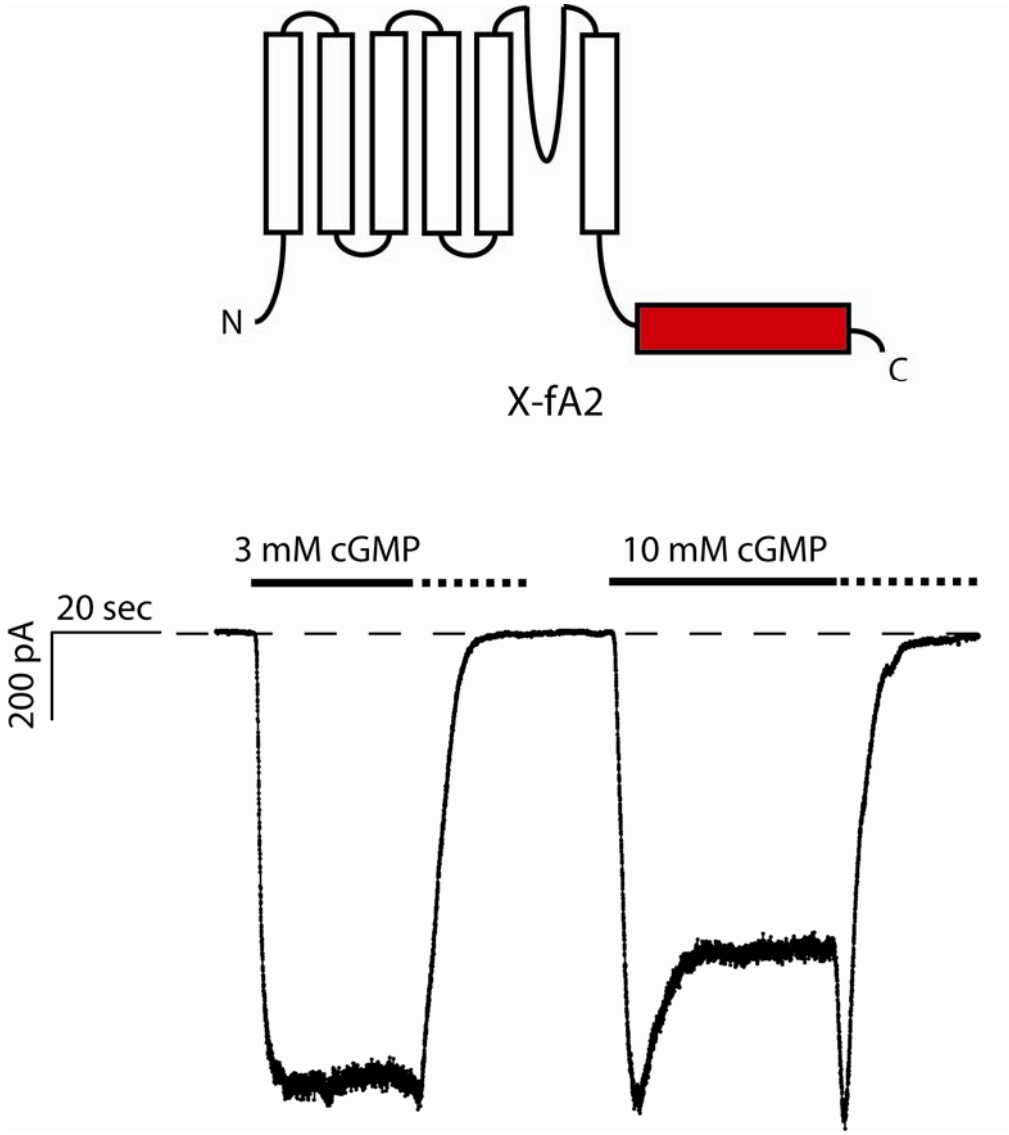

Figure 5 Composition of the X-chimera channel subunit.

The X-chimera (Young et al., 2001) was constructed from the bovine CNGA1 subunit drawn in thin lines. In the X-chimera, the N-S2 region and the pore region drawn with thick lines were substituted from the catfish CNGA2 subunit to ensure robust channel activation and single channel conductance. In the X-chimera construct series, the binding domain shown as the rectangle is varied from construct to construct.

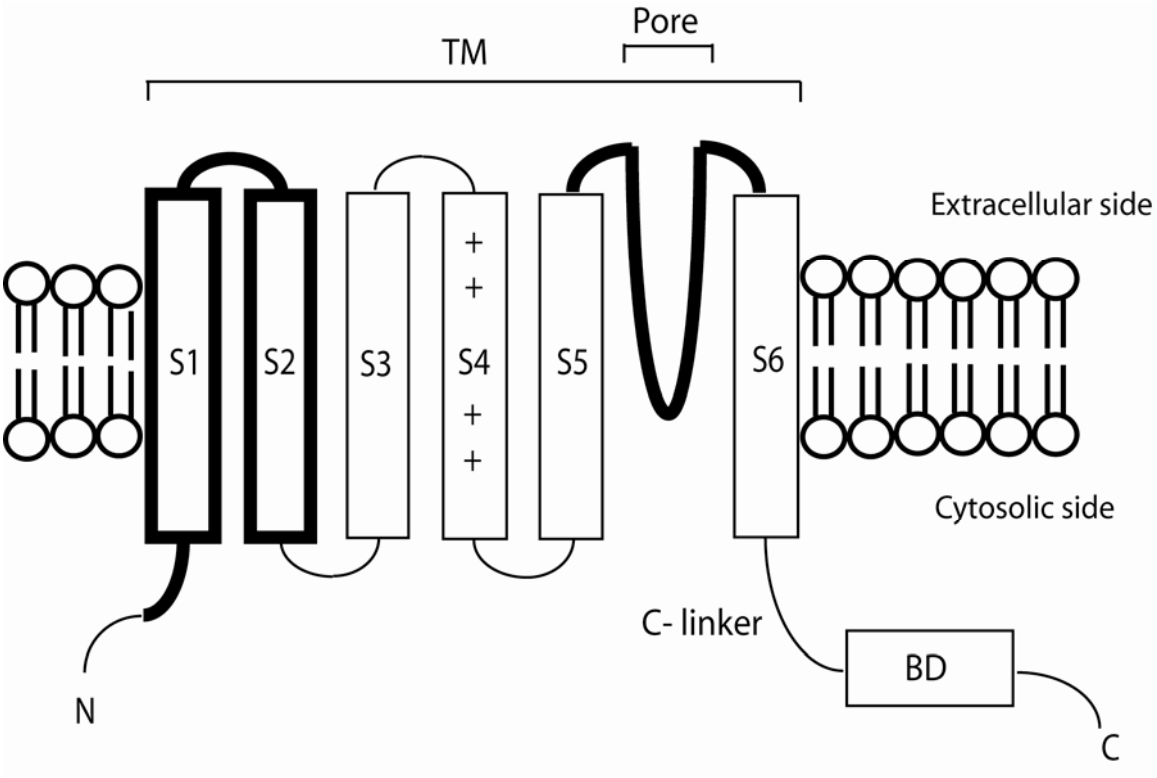

Figure 6 Tandem oligomers construction.

Tandem oligomers were constructed using standard restriction digest and ligation protocols. The letter B coloured in red represent the bimodal subunit X-fr532 and the letter N coloured in blue represent the normal subunit X-rA4. The letters E, P and H represent the EagI, PspOMI and HindIII restriction sites, respectively. EagI and PspOMI have compatible overhangs that can be re-ligated, but the re-ligated junction is resistant to EagI and PspOMI cleavage.

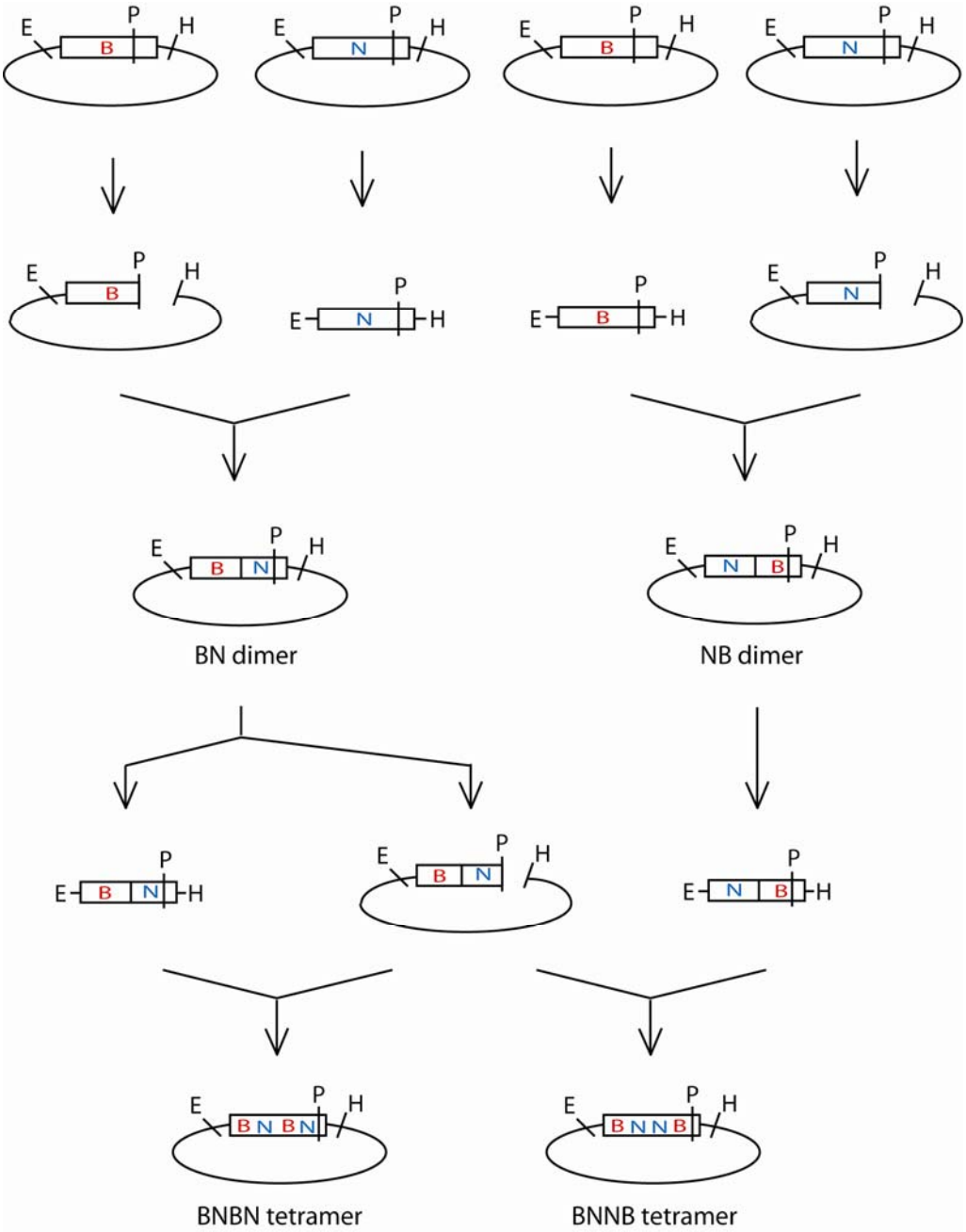

Figure 7 Restriction digest confirmed the BN tandem dimer composition.

The BN tandem dimer construct is shown on the left. The red box represents the bimodal X-fr532 pseudo-subunit coding sequence and the blue box represents the normal X-rA4 pseudo-subunit coding sequence. The line represents the pGEM-HE vector sequence. The unique XbaI restriction site is located in the vector sequence. The bimodal pseudo-subunit contains a unique EcoRV restriction site. The BN tandem dimer was double digested with XbaI and EcoRV overnight. The restriction fragments were separated in 1% agarose gel at 125 volt. The double digest yielded two expected restriction fragments shown in lane 1. The XbaI single digested sample is shown in lane 2. The undigested sample is shown in lane 3. The 1 kb molecular weight marker is shown in lane 4.

Figure 8 Restriction digest confirmed the NB tandem dimer composition.

The NB tandem dimer construct is shown on the right. The red box represents the bimodal X-fr532 pseudo-subunit coding sequence and the blue box represents the normal X-rA4 pseudo-subunit coding sequence. The line represents the pGEM-HE vector sequence. The unique NotI restriction site is located in the vector sequence. The bimodal pseudo-subunit contains a unique EcoRV restriction site. The NB tandem dimer was double digested with NotI and EcoRV overnight. The restriction fragments were separated in 1% agarose gel at 125 volt. The double digest yielded two expected restriction fragments shown in lane 6. The NotI single digested sample is shown in lane 8. The undigested sample is shown in lane 9. The 1 kb molecular weight marker is shown in lane 5. The 100 bp molecular weight marker is shown in lane 7.

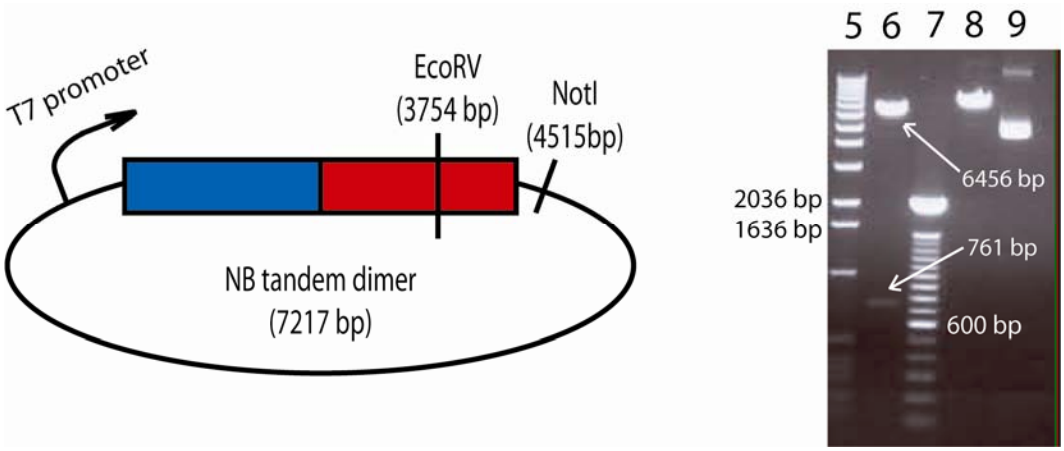

Figure 9 Restriction digest confirmed the BNBN tandem tetramer composition.

The BNBN tandem tetramer construct is shown on top. The red boxes represent the bimodal X-fr532 pseudo-subunits and the blue boxes represent the normal X-rA4 pseudo-subunits. The line represents the pGEM-HE vector sequence. The unique XbaI restriction site is located in the vector sequence. Each bimodal pseudo-subunit contains a unique EcoRV restriction site. The BNBN tandem tetramer was double digested with XbaI and EcoRV overnight. The restriction fragments are separated in 1% agarose gel at 125 volt. The double digest yielded three expected restriction fragments shown in lane1. The 1 kb molecular weight marker is shown in lane 2.

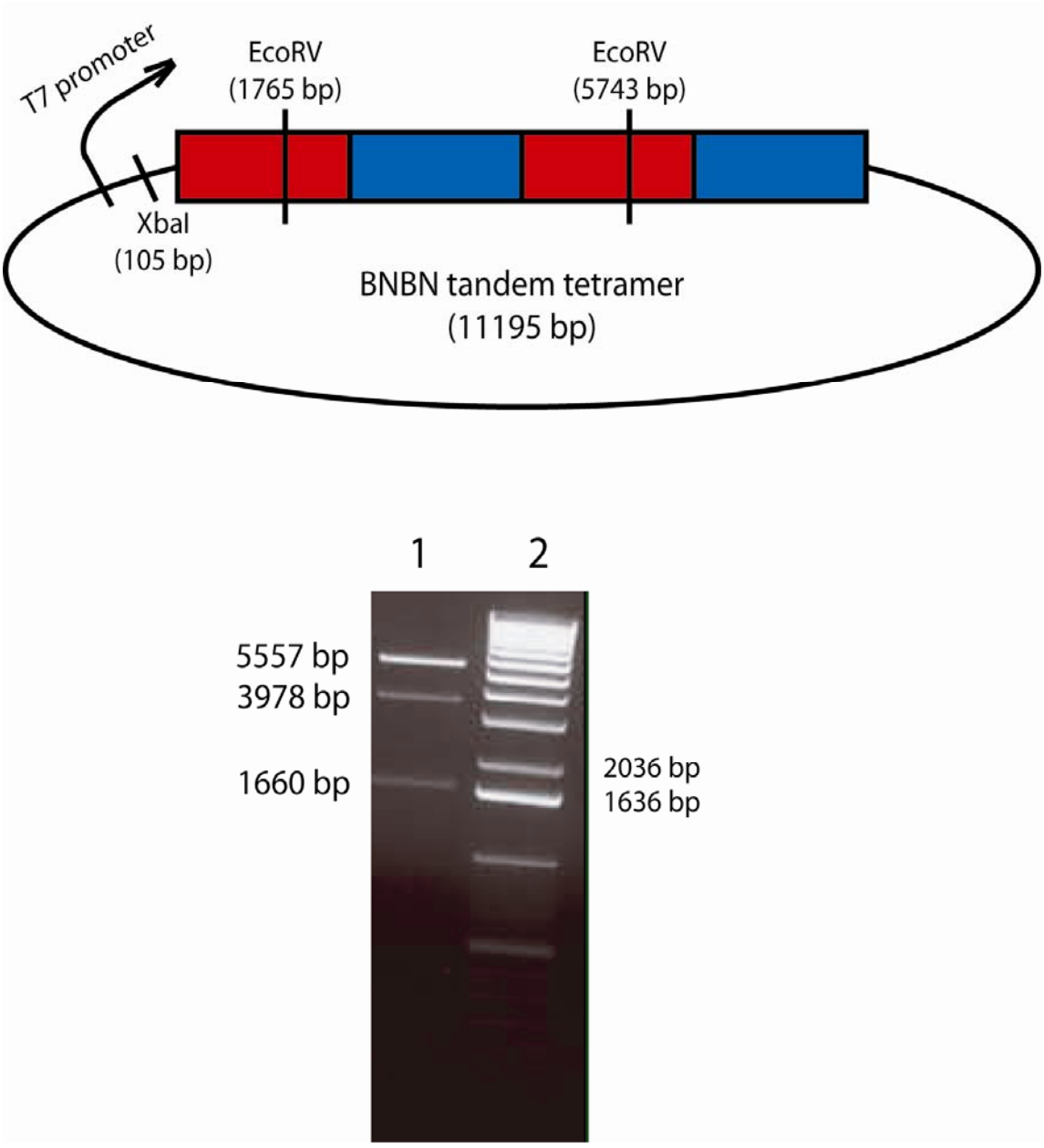

Figure 10 Restriction digest confirmed the BNNB tandem tetramer composition.

The BNNB tandem tetramer construct is shown on top. The red boxes represent the bimodal X-fr532 pseudo-subunits and the blue boxes represent the normal X-rA4 pseudo-subunits. The line represents the pGEM-HE vector sequence. The unique XbaI restriction site is located in the vector sequence. Each bimodal pseudo-subunit contains a unique EcoRV restriction site. The BNNB tandem tetramer was double digested with XbaI and EcoRV overnight. The restriction fragments are separated in 1% agarose gel at 125 volt. The double digest yielded three expected restriction fragments shown in lane 3. The undigested sample is shown in lane 2. The 1 kb molecular weight marker is shown in lane 1.

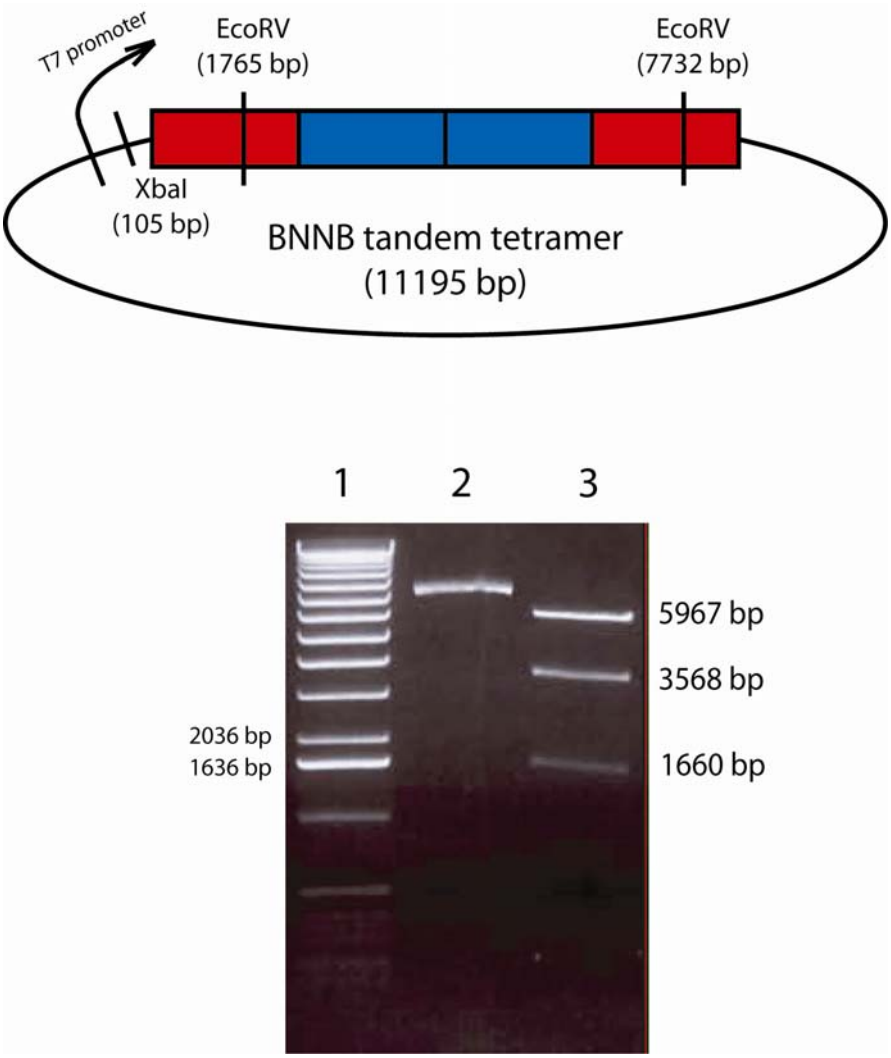

Figure 11 Tandem oligomers cRNA separated on denaturing gel electrophoresis.

The tandem oligomer constructs were linearized and transcribed into cRNA. The cRNA were separated in 1.2% denaturing agarose gel at 130 volt. X-fA2 is a monomer. BN and NB are tandem dimers with two pseudo-subunits. BNBN and BNNB are tandem tetramers with four pseudo-subunits.

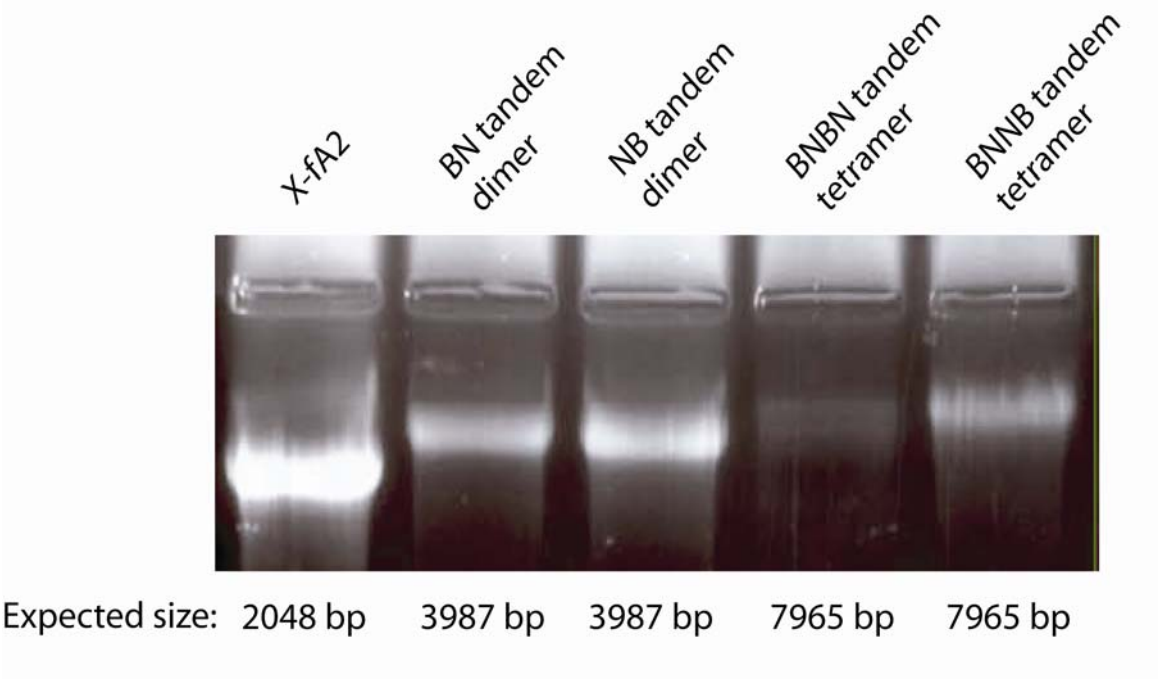

Figure 12 Bimodal activities of the X-chimera series.

All channel sequences outside the BD are identical (see “Molecular subcloning of the X-chimera seris”, section 3.2). All constructs were expressed as homomers and tested with the excised patch-clamp. The construct is bimodal if the $I_{10mMcGMP}/I_{3mMcGMP}$ current ratio is below 0.95. The $P_{o10mMcGMP}/P_{o3mMcGMP}$ ratio and by extension the $I_{10mMcGMP}/I_{3mMcGMP}$ ratio of X-fr561 was obtained from previous studies (Young et al., 2001). The asterisk marks the F510Y substitution in X-fr496b. Errors are standard deviations and N is the number of recordings.

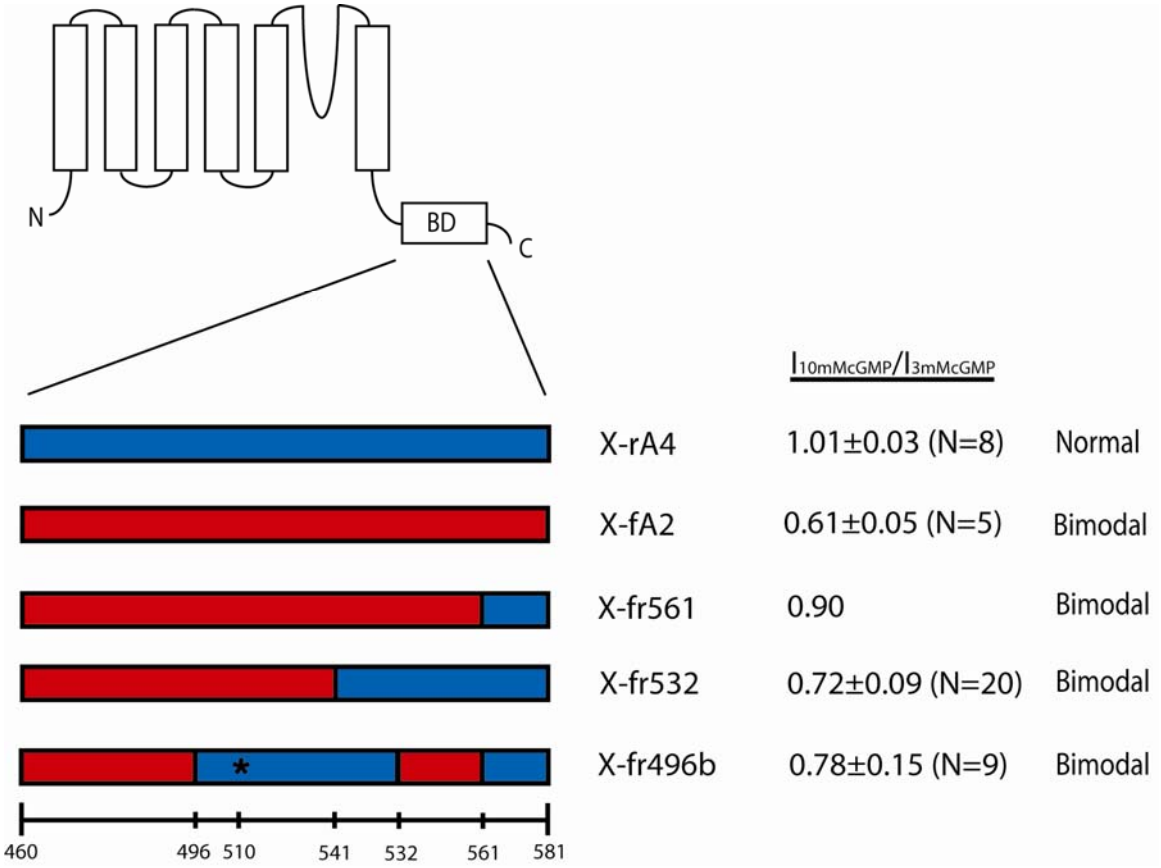

Figure 13 Sample current trace from the normal channel X-rA4.

Messenger RNA *in vitro* transcribed from the plasmid containing X-rA4 was injected into *Xenopus* oocytes to express X-rA4 as homomers. Activities from X-rA4 were recorded using the excised patch-clamp technique. The patch voltage was held constant at -40 mV. Cyclic-GMP enriched bath solutions were perfused to the membrane patch with a gravity flow perfusion system to activate the channels. The solid line represents the presence of cGMP and the dotted line represents the cGMP wash out. The dash line marks the zero current level.

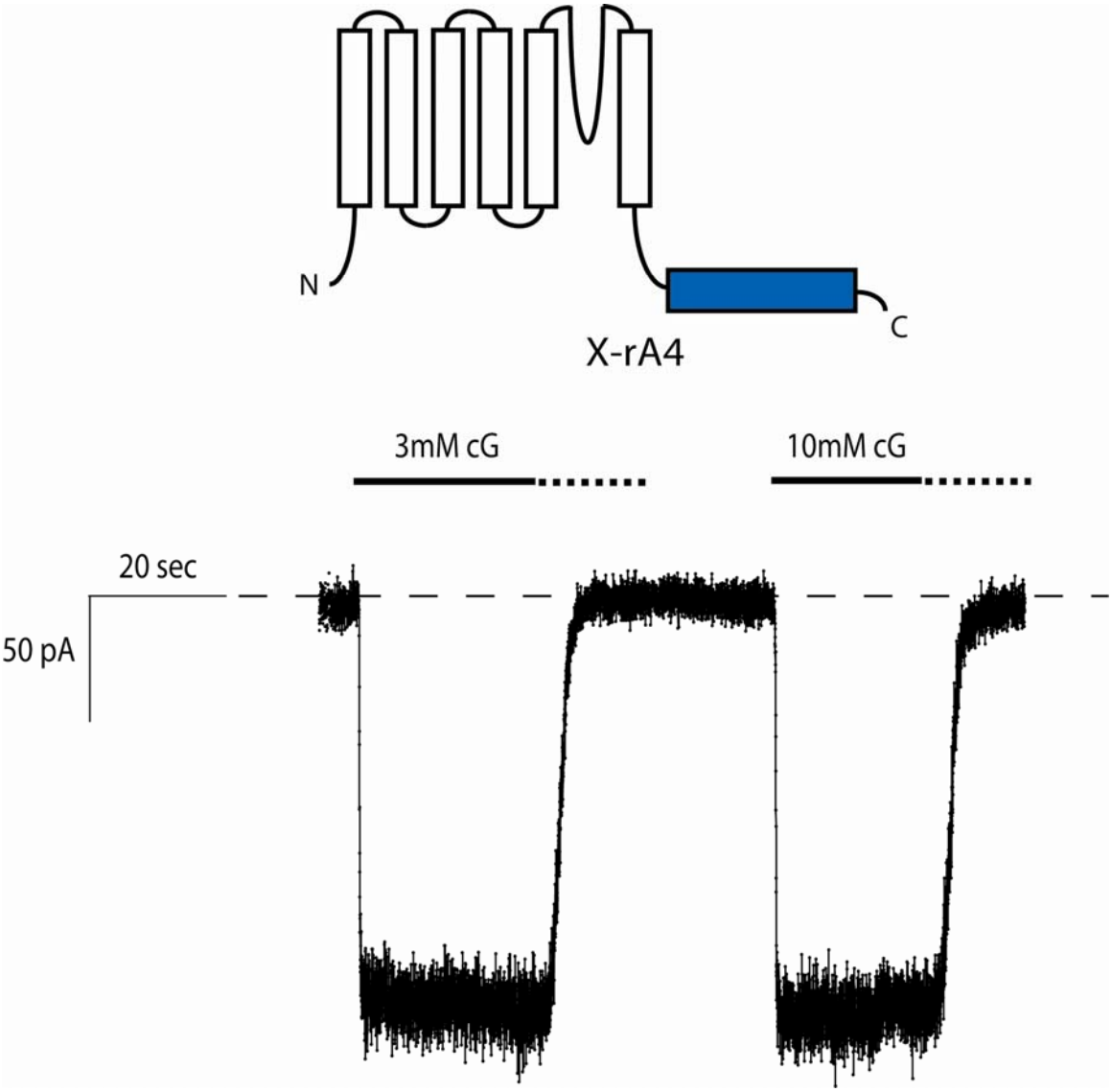

Figure 14 Cyclic nucleotide binding domains sequence alignment.

The cyclic nucleotide binding domain (BD) sequences from the A-helix to the C-helix from the mouse HCN2, catfish olfactory CNGA2, rat olfactory CNGA4, BD chimera fr532 and BD chimera fr496b are aligned with the ClustalW2 program (Larkin et al., 2007) with default settings. The cGMP contacting residues identified from the solved HCN2 BD crystal structure (Zagotta et al., 2003) and their homologous residues in the CNGA2 and CNGA4 BD are highlighted in orange. Residues unique to the CNGA2 BD are coloured red and residues unique to the CNGA4 are coloured blue. The rectangles represent alpha helices, arrows represent beta strands and the lines represent loops. The secondary structural assignments were adapted from the solved HCN2 BD crystal structure (Zagotta et al., 2003).

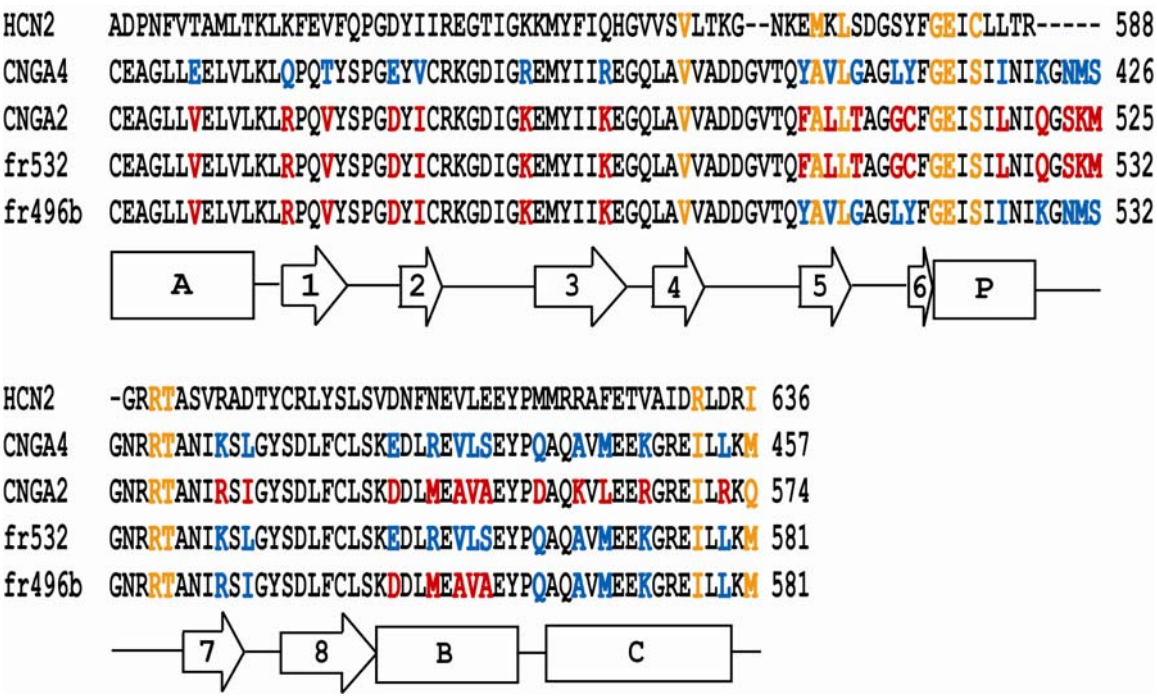

Figure 15 Sample current trace from the bimodal channel X-fr532.

Messenger RNA *in vitro* transcribed from the plasmid containing X-fr532 was injected into *Xenopus* oocytes to express X-fr532 as homomers. The fr532 BD contains CNGA2 sequence from A-helix to the β7 and CNGA4 sequence from the end of β7 to the end of C-helix. Activities from X-fr532 were recorded using the excised patch-clamp technique. The patch voltage was held constant at -40 mV. Cyclic-GMP enriched bath solutions were perfused to the membrane patch with a gravity flow perfusion system to activate the channels. The solid line represents the presence of cGMP and the dotted line represents the cGMP wash out. The dash line marks the zero current level.

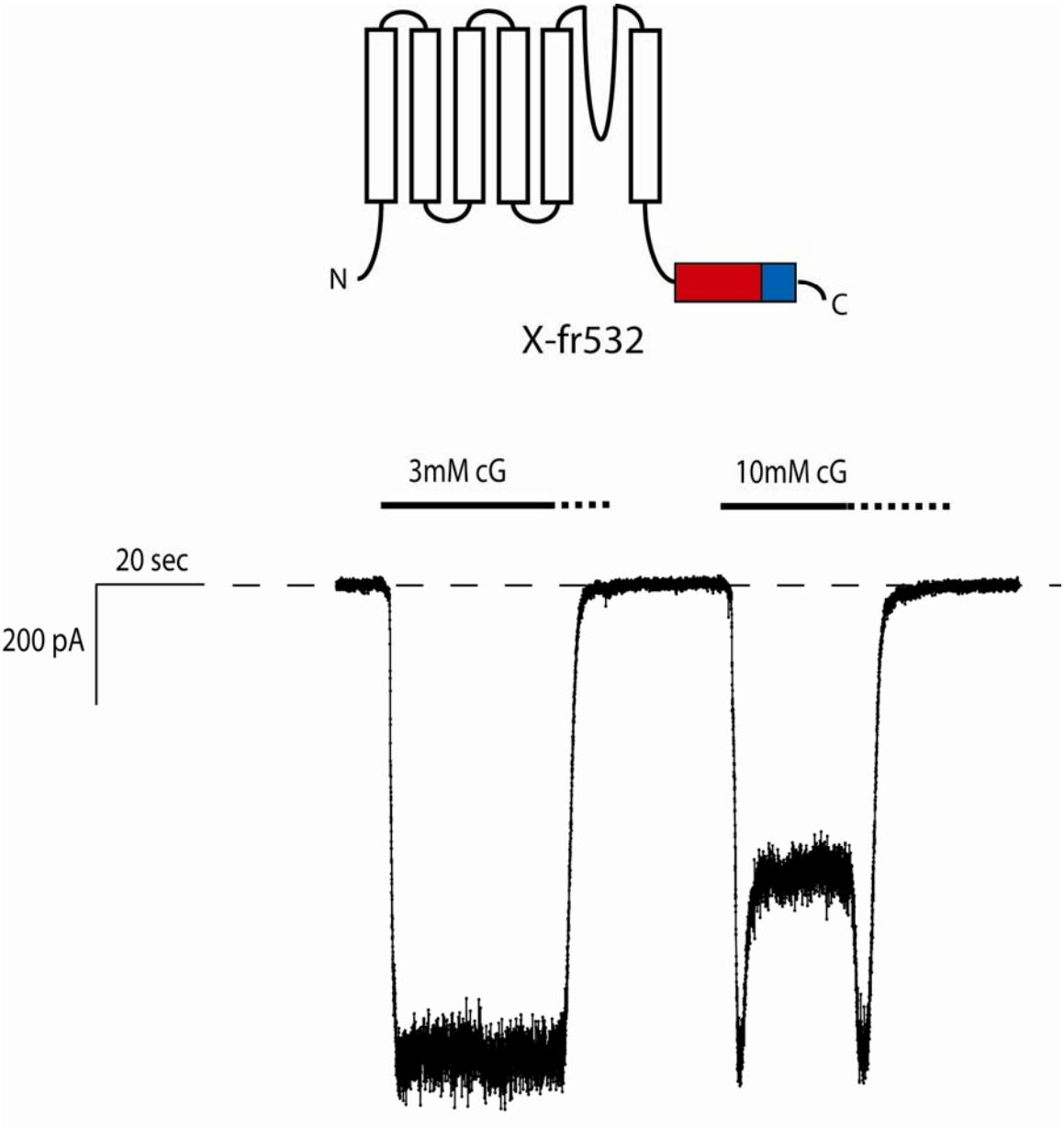

Figure 16 Sample current trace from the bimodal channel X-fr496b.

Messenger RNA *in vitro* transcribed from the plasmid containing X-fr496b was injected into *Xenopus* oocytes to express X-fr496b as homomers. The fr496b BD contains CNGA2 sequence from A-helix to the end of β3 and the B-helix. The fr496b BD also contains CNGA4 sequence from the end of β3 to the beginning of the B-helix and the C-helix. Activities from X-fr496b were recorded using the excised patch-clamp technique. The patch voltage was held constant at -40 mV. Cyclic-GMP enriched bath solutions were perfused to the membrane patch with a gravity flow perfusion system to activate the channels. The solid line represents the presence of cGMP and the dotted line represents the cGMP wash out. The dash line marks the zero current level.

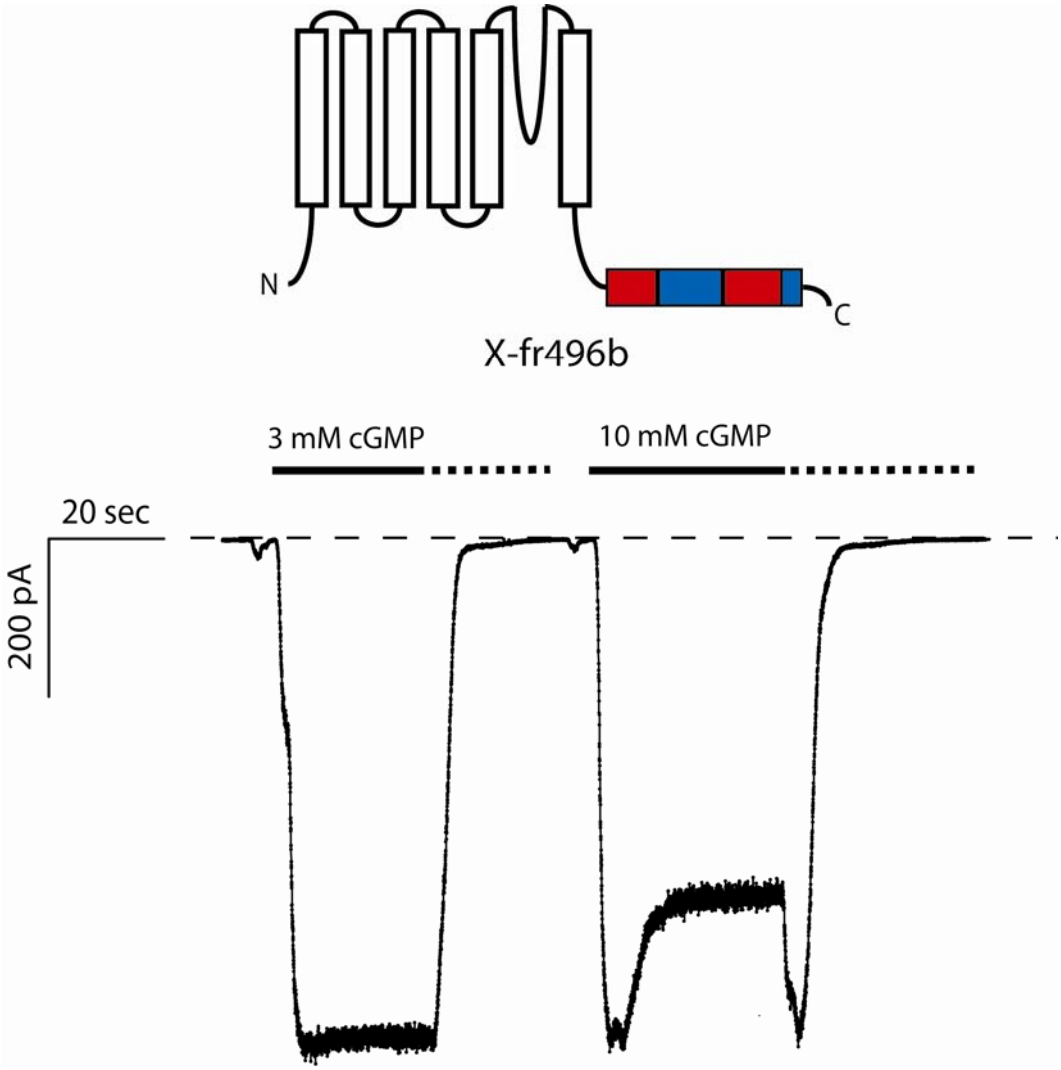

Figure 17 Superimposition of the binding domain comparative models.

Three dimensional structures of the CNGA2 BD (red), CNGA4 BD (blue) and CNGA2F510Y (green) were predicted and superimposed. The loop deviation sensitive to the F510Y *in silica* mutation is boxed. The amino and carboxyl terminus are marked with N and C.

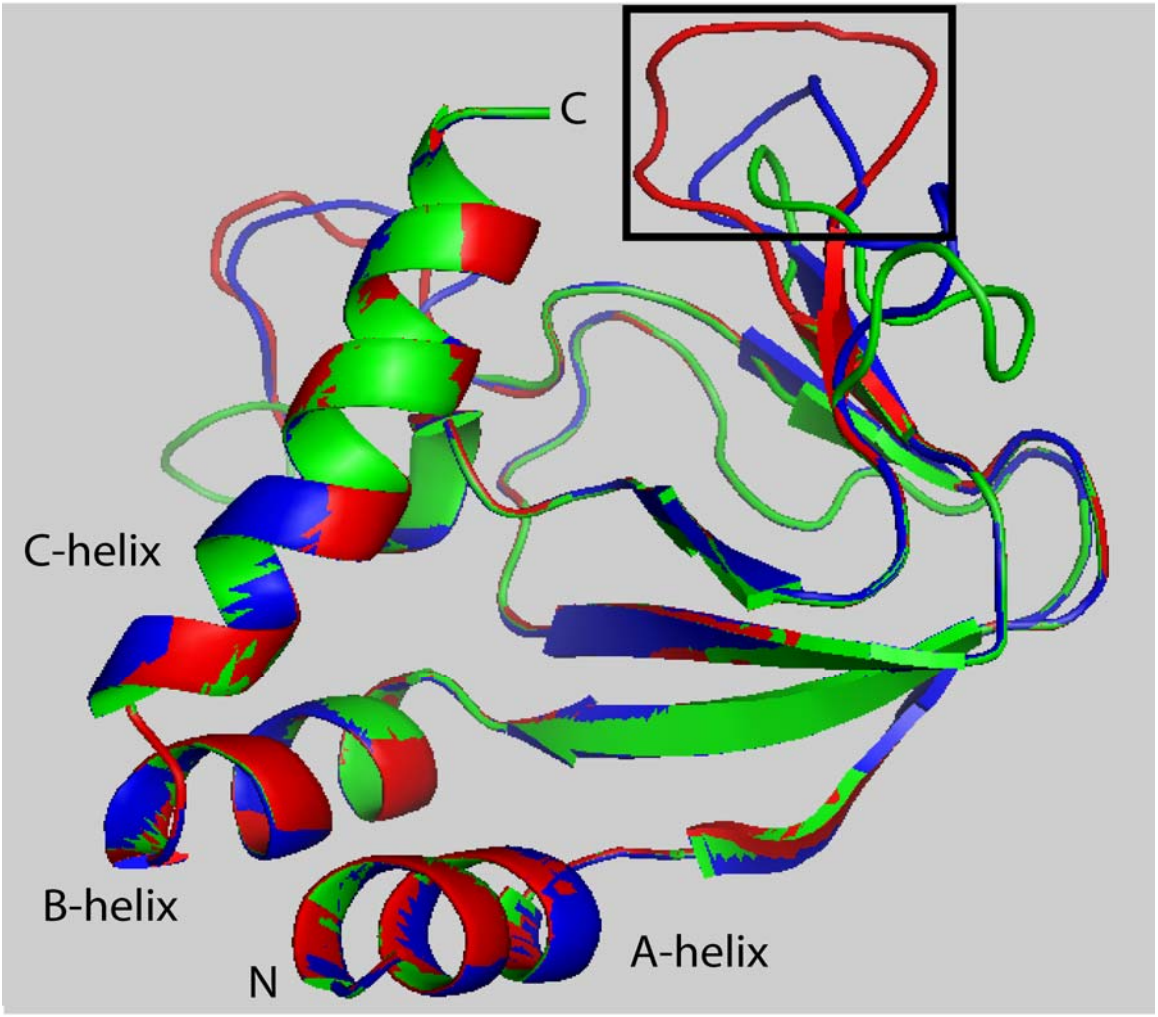

Figure 18 Dose-response curve of the bimodal channel X-fr532.

Macroscopic steady state currents activated with cGMP (open circle) and cAMP (closed circle) measured at -40 mV were normalized to macroscopic steady state current activated with 3 mM cGMP. Points plot means and error bars are standard deviations (3 to 20 patches for each data point).

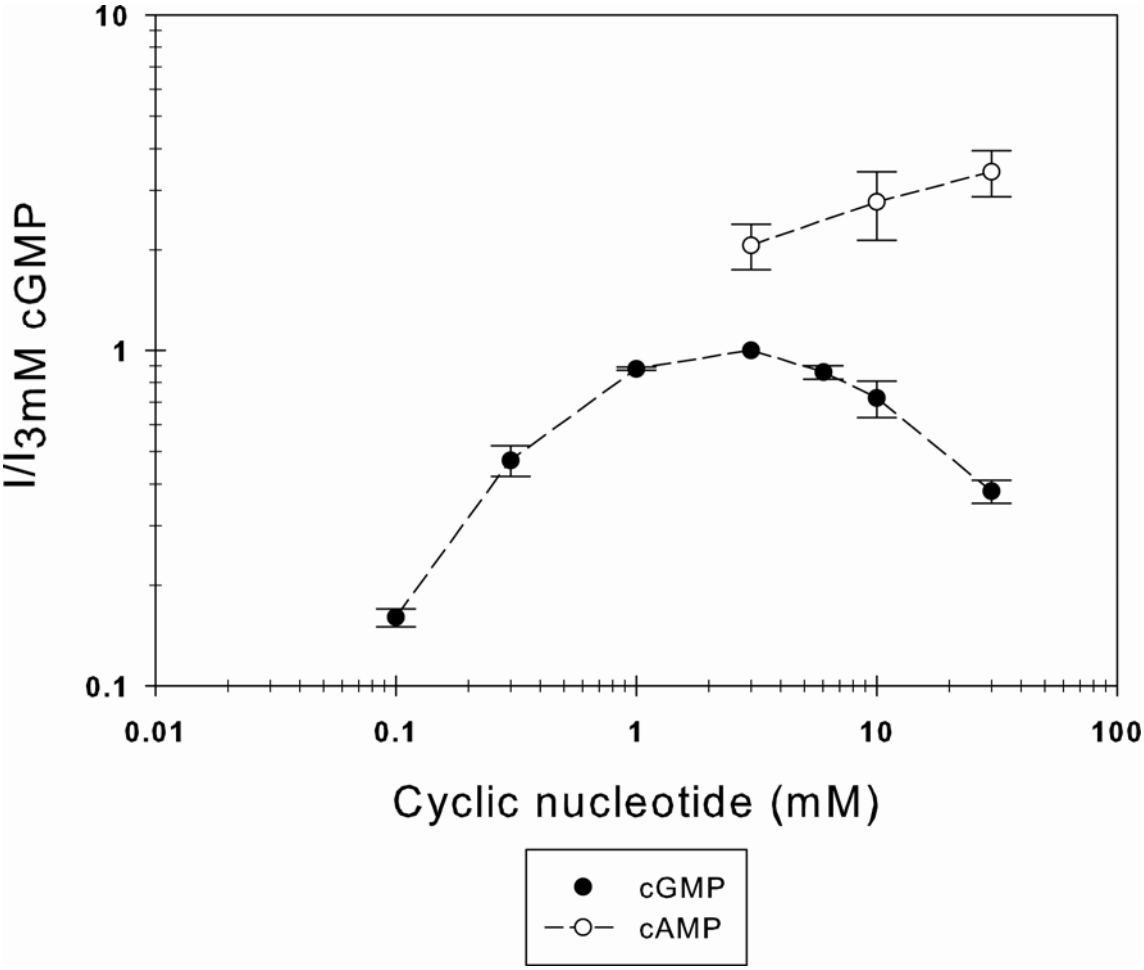

Figure 19 The expected BN tandem dimer assembly.

The pseudo-subunit labeled B represents the bimodal X-fr532. The pseudo-subunit labeled N represents the normal X-rA4. When expressed as homomer, two BN dimers are expected to assemble into a functional channel with two bimodal subunits and two normal subunits arranged diagonally opposite to each other (*trans*).

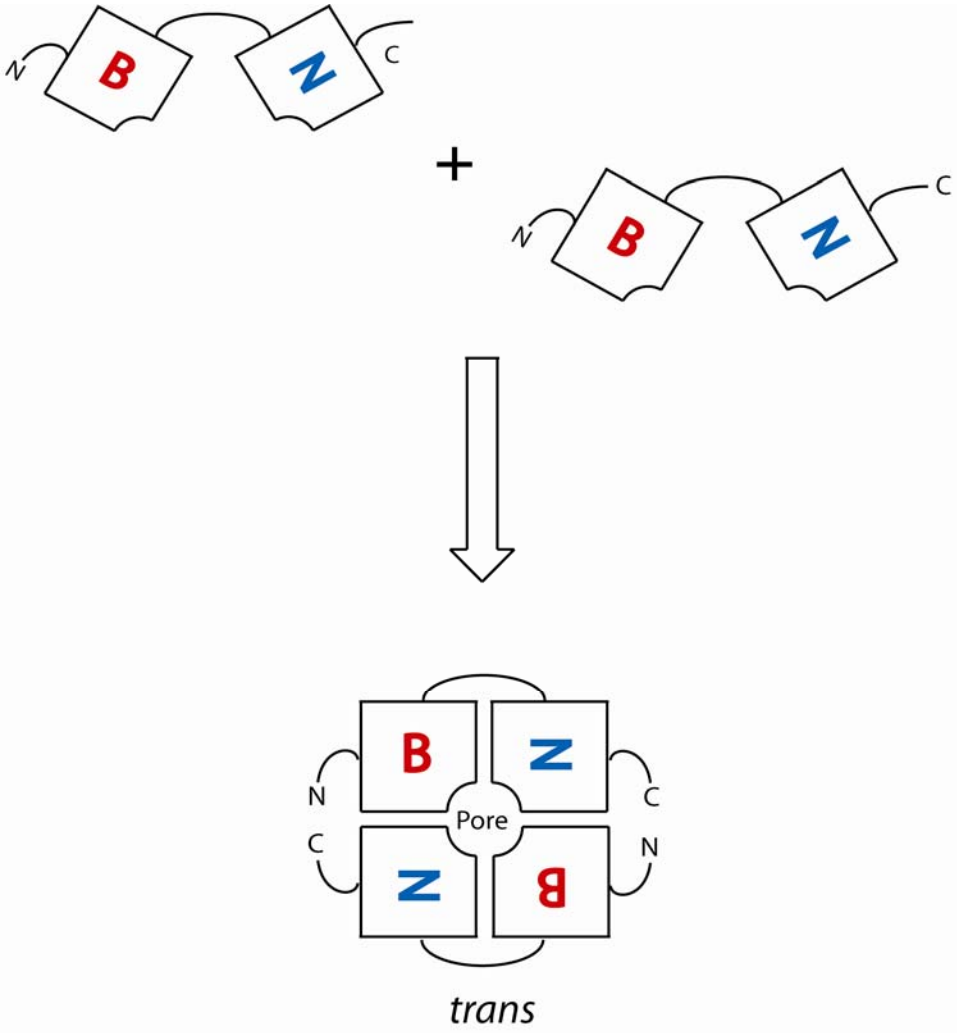

Figure 20 The expected NB tandem dimer assembly.

The pseudo-subunits labelled N represent the normal X-rA4. The pseudo-subunits labelled B represent the bimodal X-fr532. When expressed as homomer, two NB tandem dimers are expected to assemble into a functional channel with two bimodal subunits and two normal subunits arranged diagonally opposite to each other (*trans*).

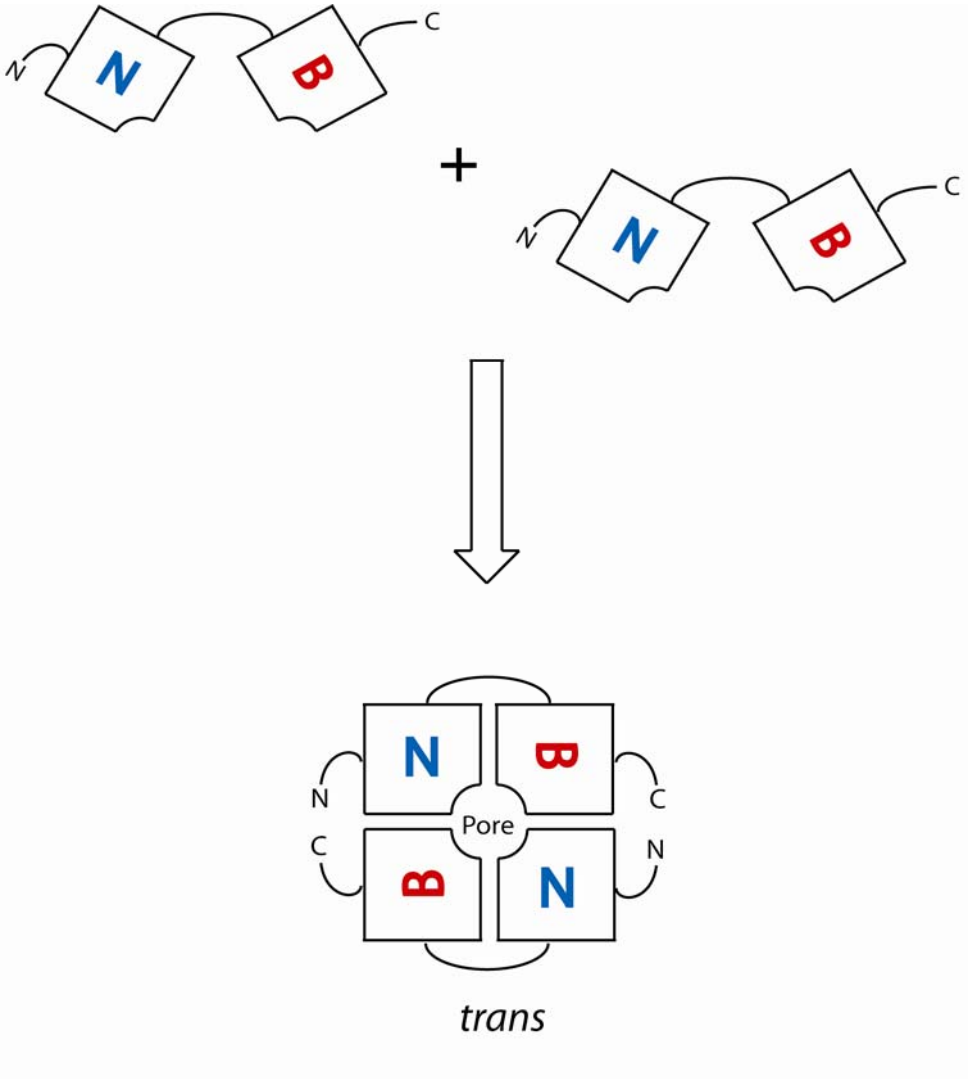

Figure 21 The expected assembly for BN and NB tandem dimer co-expression.

When the BN and the NB dimers are co-expressed in equal amount, two dimers of either kind are expected to assemble into a functional channel with two bimodal subunits and two normal subunits. The two bimodal subunits and two normal subunits are arranged either diagonally opposite to each other (*trans*) or adjacent to each other (*cis*).

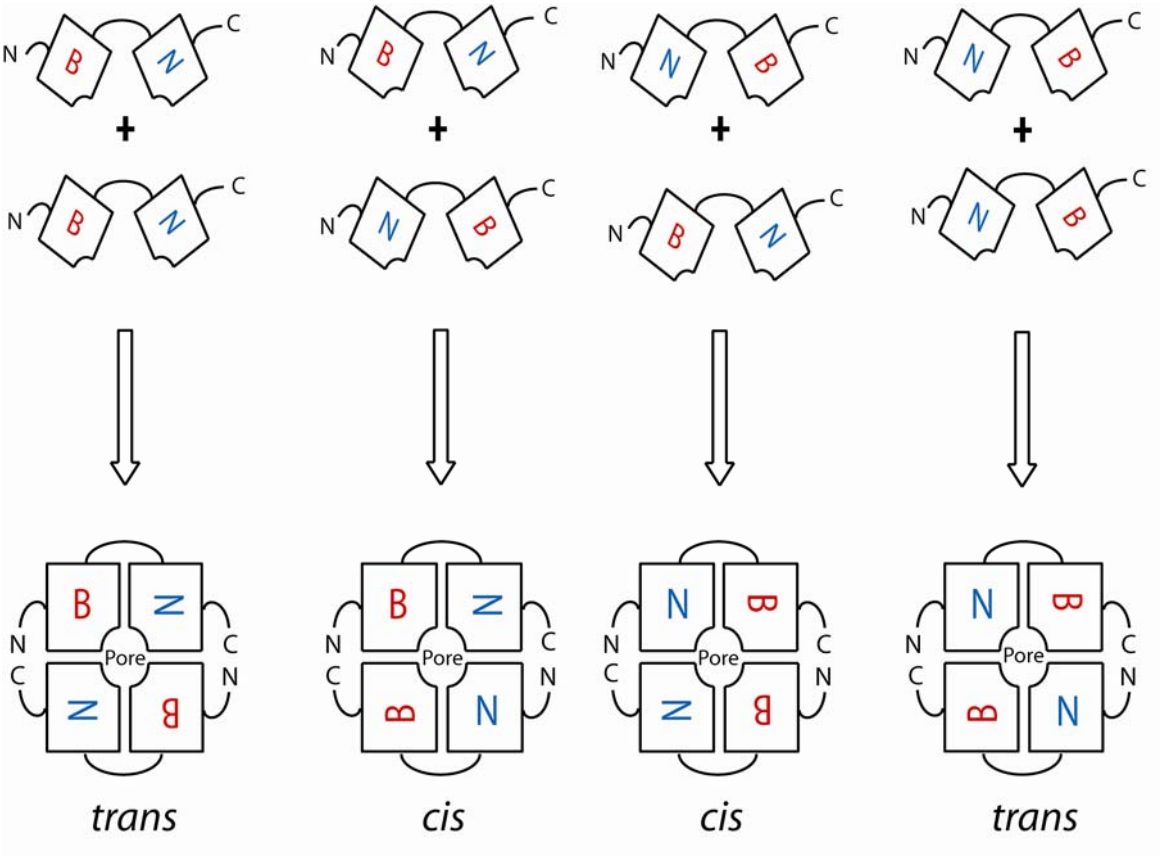

Figure 22 The expected BNBN tandem tetramer assembly.

The BNBN tetramer contains four pseudo-subunits. The pseudo-subunit labeled B represents the bimodal X-fr532. The pseudo-subunit labeled N represents the normal X-rA4. When expressed alone, each copy of the BNBN tetramer is expected to fold into a functional channel with its two bimodal pseudo-subunits arranged diagonally opposite to each other (trans).

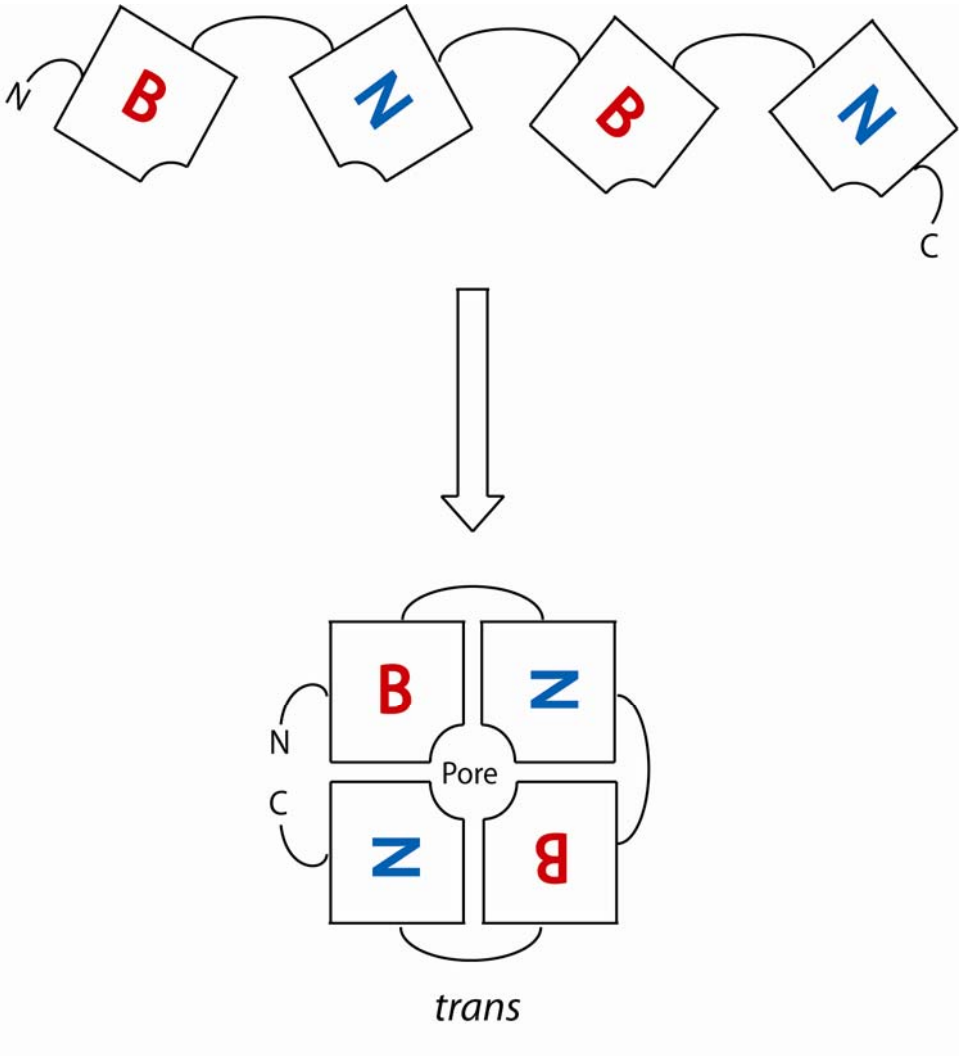

Figure 23 Sample current trace of the BNBN tandem tetramer.

Messenger RNA in vitro transcribed from the plasmid containing BNBN tetramer was injected into *Xenopus* ooctyes to express BNBN tetramer alone. Activities from the BNBN tetramer were recorded using the excised patch-clamp technique. The patch voltage was held constant at -40 mV. Cyclic-GMP enriched bath solutions were perfused to the membrane patch with a gravity flow perfusion system to activate the channels. The solid line represents the presence of cGMP and the dotted line represents the cGMP wash out. The dash line marks the zero current level.

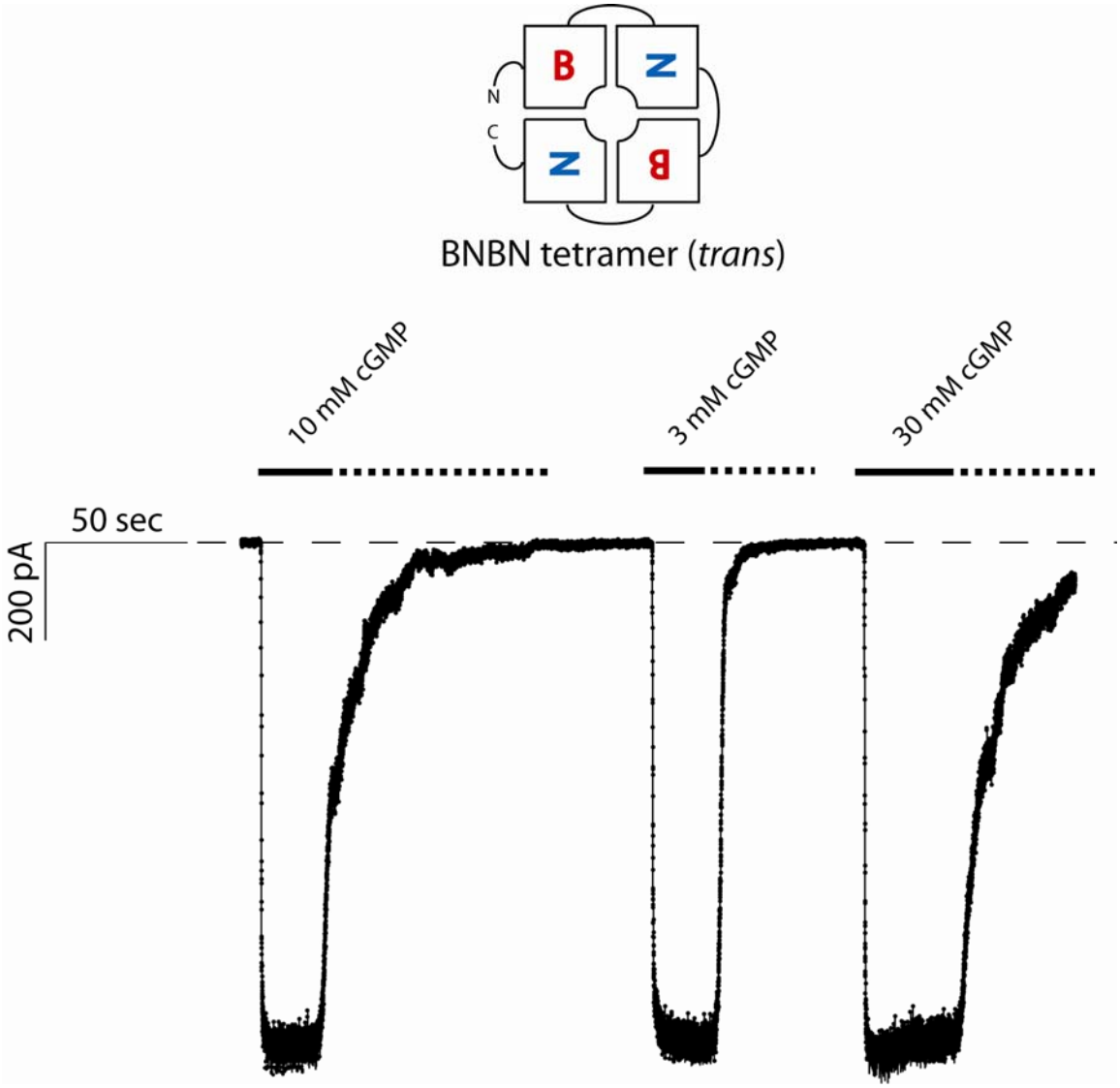

Figure 24 Dose-response curve of the BNBN tandem tetramer.

Macroscopic steady state currents activated with cGMP (open circle) and cAMP (closed circle) measured at -40 mV were normalized to macroscopic steady state current activated with 3 mM cGMP. Points plot means and error bars are standard deviations (4 to 13 patches for each data point).

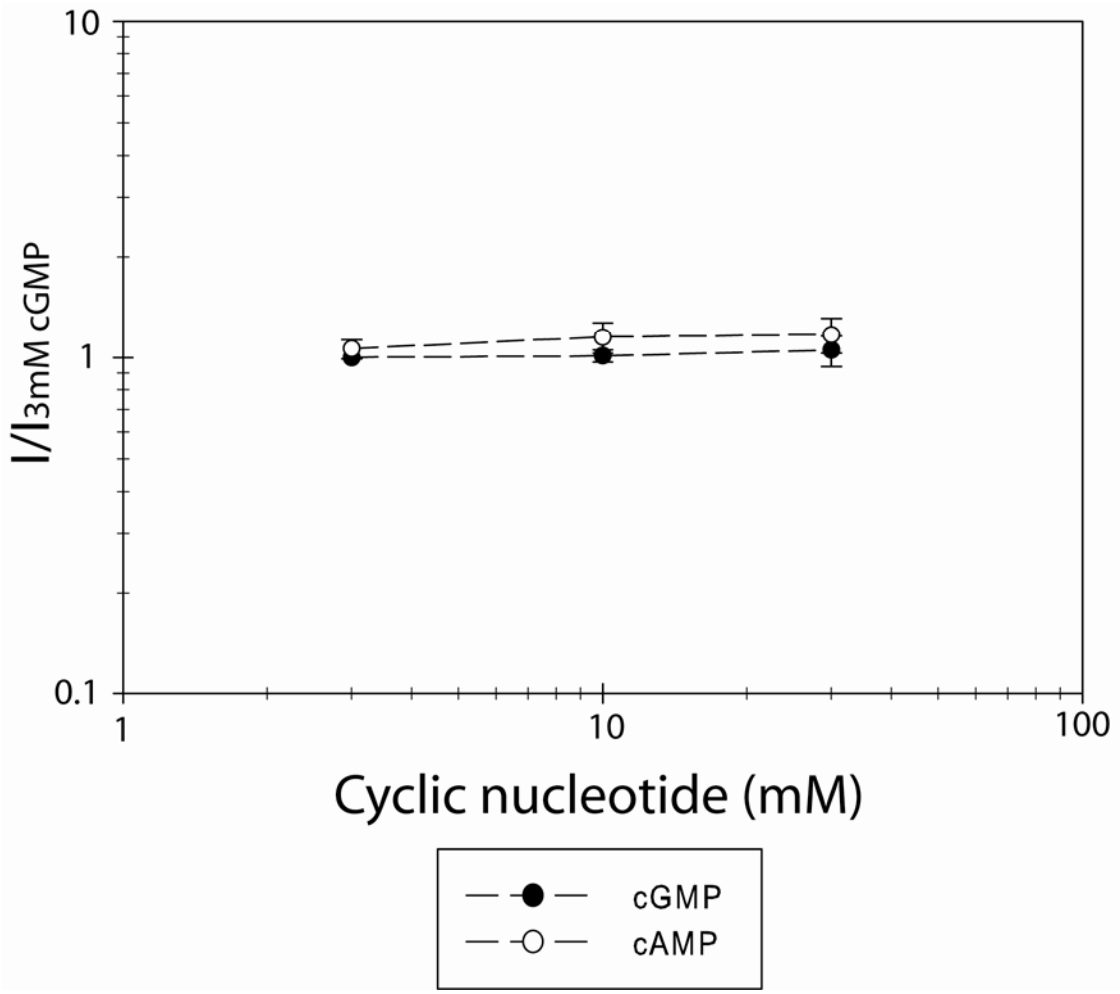

Figure 25 The expected BNNB tandem tetramer assembly.

The BNNB tetramer contains four pseudo-subunits. The pseudo-subunits labelled B represent the bimodal X-fr532. The pseudo-subunits labelled N represent the normal X-rA4. When expressed alone, each copy of the BNNB tetramer is expected to fold into a functional channel with its two bimodal pseudo-subunits arranged adjacent to each other (cis).

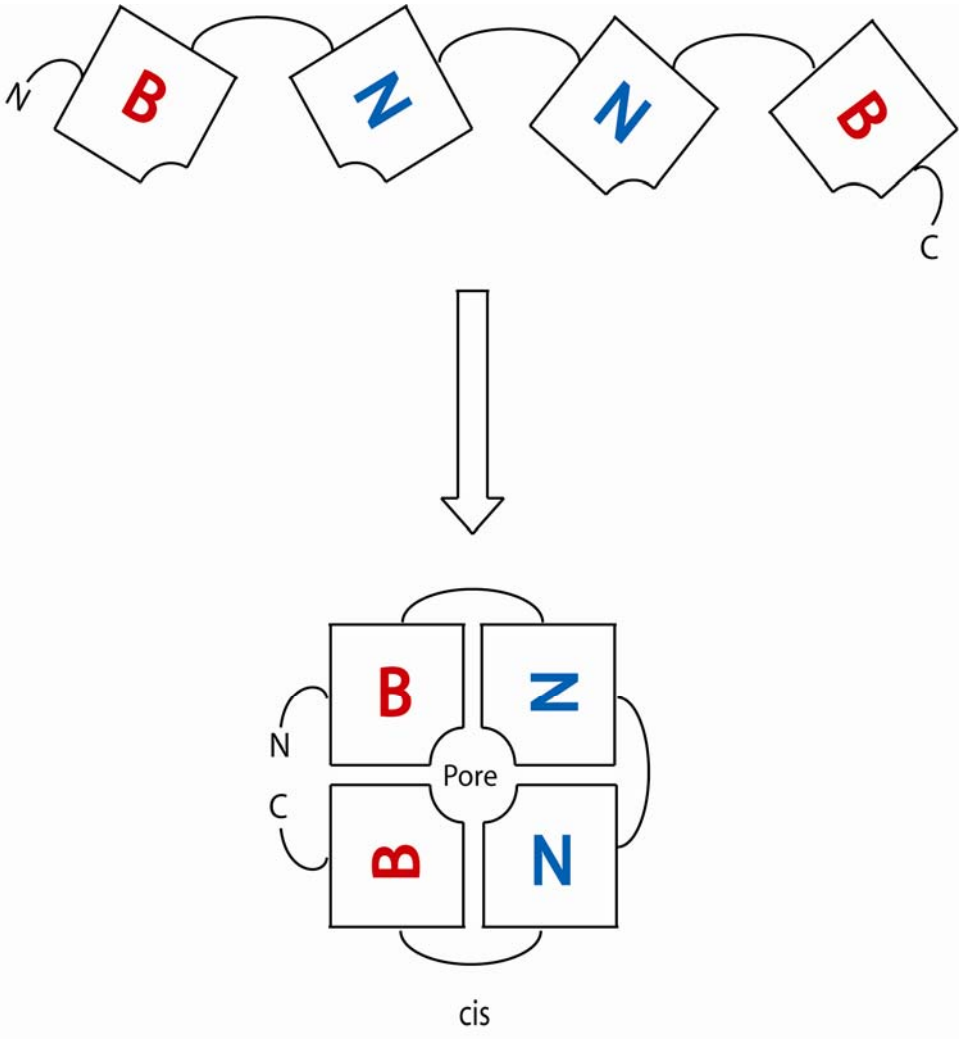

Figure 26 Sample current trace of the BNNB tandem tetramer.

Messenger RNA in vitro transcribed from the plasmid containing BNNB tetramer was injected into *Xenopus* ooctyes to express BNNB tetramer alone. Activities from the BNNB tetramer were recorded using the excised patch-clamp technique. The patch voltage was held constant at -40 mV. Cyclic-GMP enriched bath solutions were perfused to the membrane patch with a gravity flow perfusion system to activate the channels. The solid line represents the presence of cGMP and the dotted line represents the cGMP wash out. The dash line marks the zero current level.

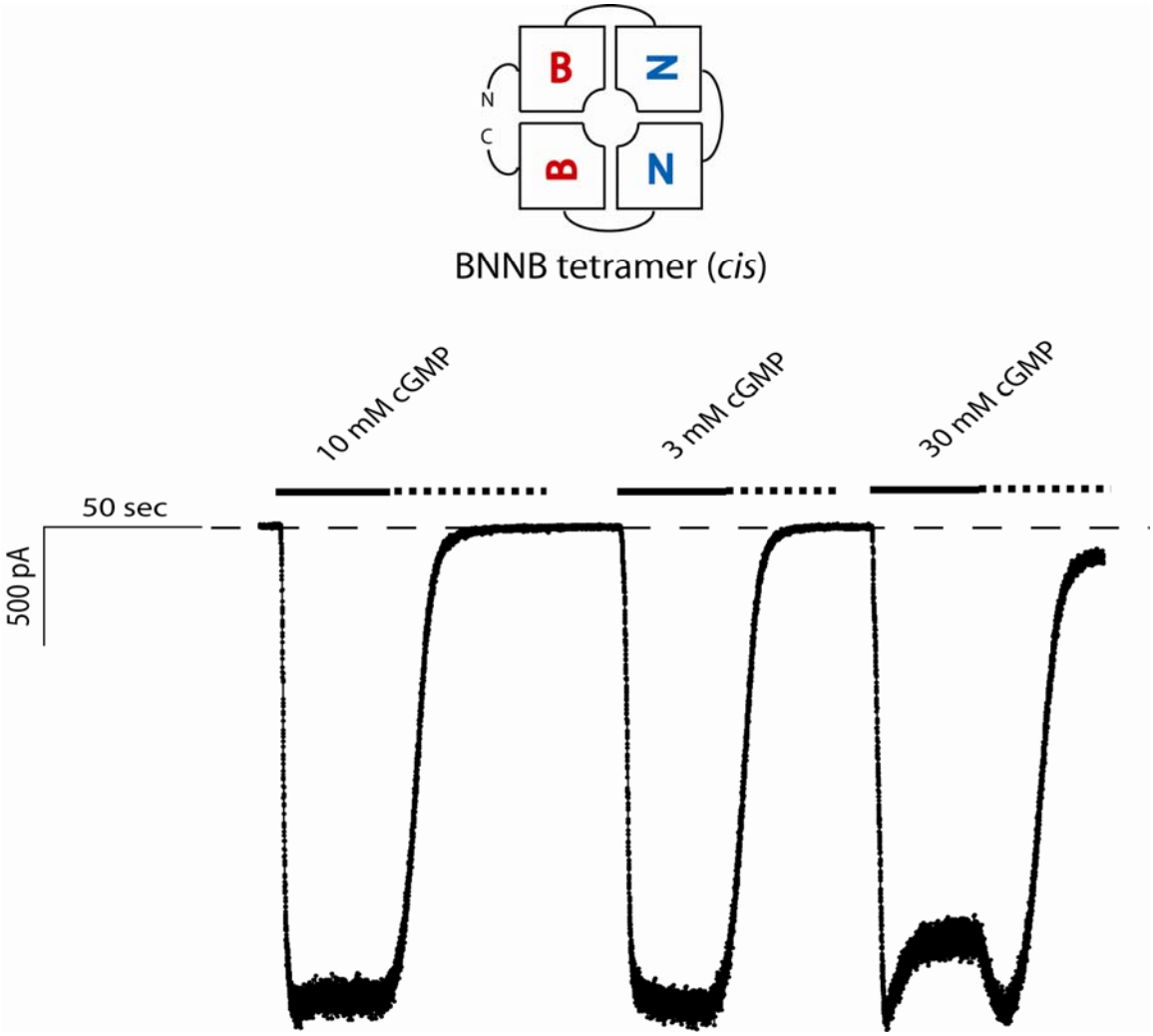

Figure 27 Dose-response curve of the BNNB tandem tetramer.

Macroscopic steady state currents activated with cGMP (open circle) and cAMP (closed circle) measured at -40 mV were normalized to macroscopic steady state current activated with 3 mM cGMP. Points plot means and error bars are standard deviations (3 to 12 patches for each data point).

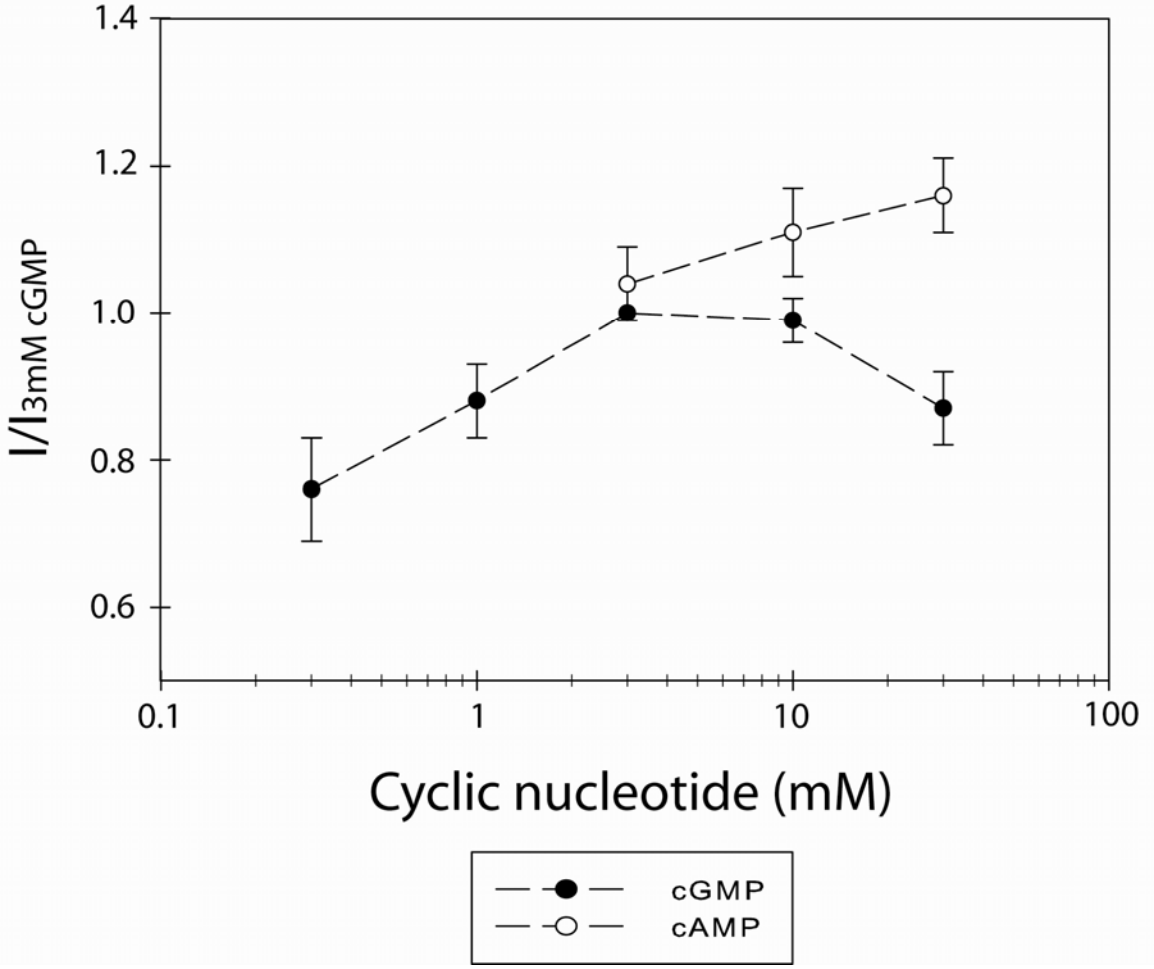

Figure 28 Dimer assembly within the coupled-dimer model.

The BNBN tetramer shown in A can have two equivalent dimer assemblies (horizontal and vertical), however all dimers have one bimodal and one normal pseudo-subunit. The BNNB tetramer shown in B can have two non-equivalent dimer assemblies (horizontal and vertical) within the coupled-dimer. In the horizontal assembly, all dimers have one bimodal and one normal pseudo-subunit. In the vertical assembly, one dimer has two bimodal pseudo-subunits and the other dimer has two normal pseudo-subunits.

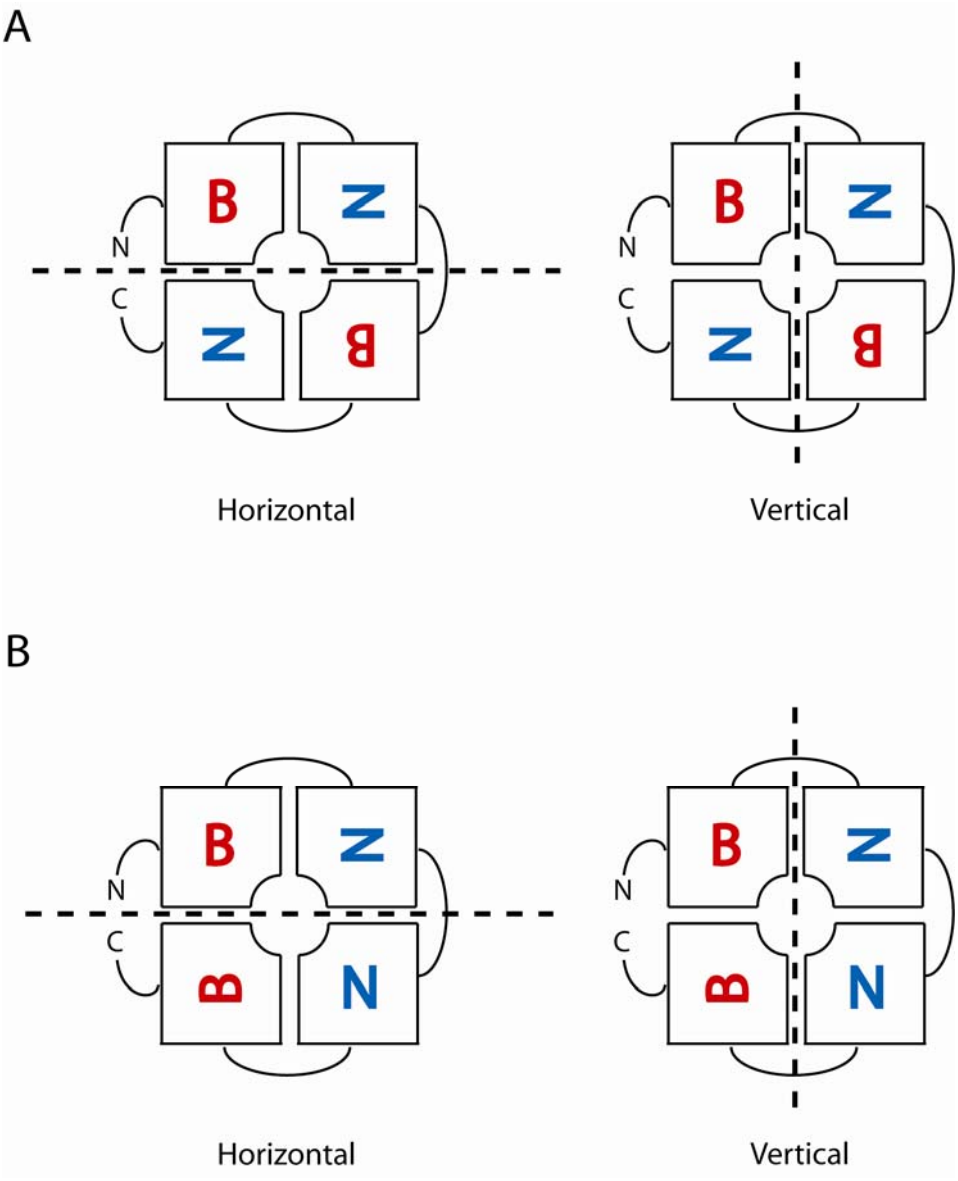

Figure 29 Bimodal binding domain tetramer viewed from the top.

Comparative model of the bimodal binding domain were predicted from the solved HCN2 binding domain crystal structure (Zagotta et al., 2003). The N-terminal region (A-helix to the end of β3) where possible critical residues are located is coloured red. The C-terminal region is coloured grey. Interface between binding domains are likely the location of the unconventional cGMP binding site.

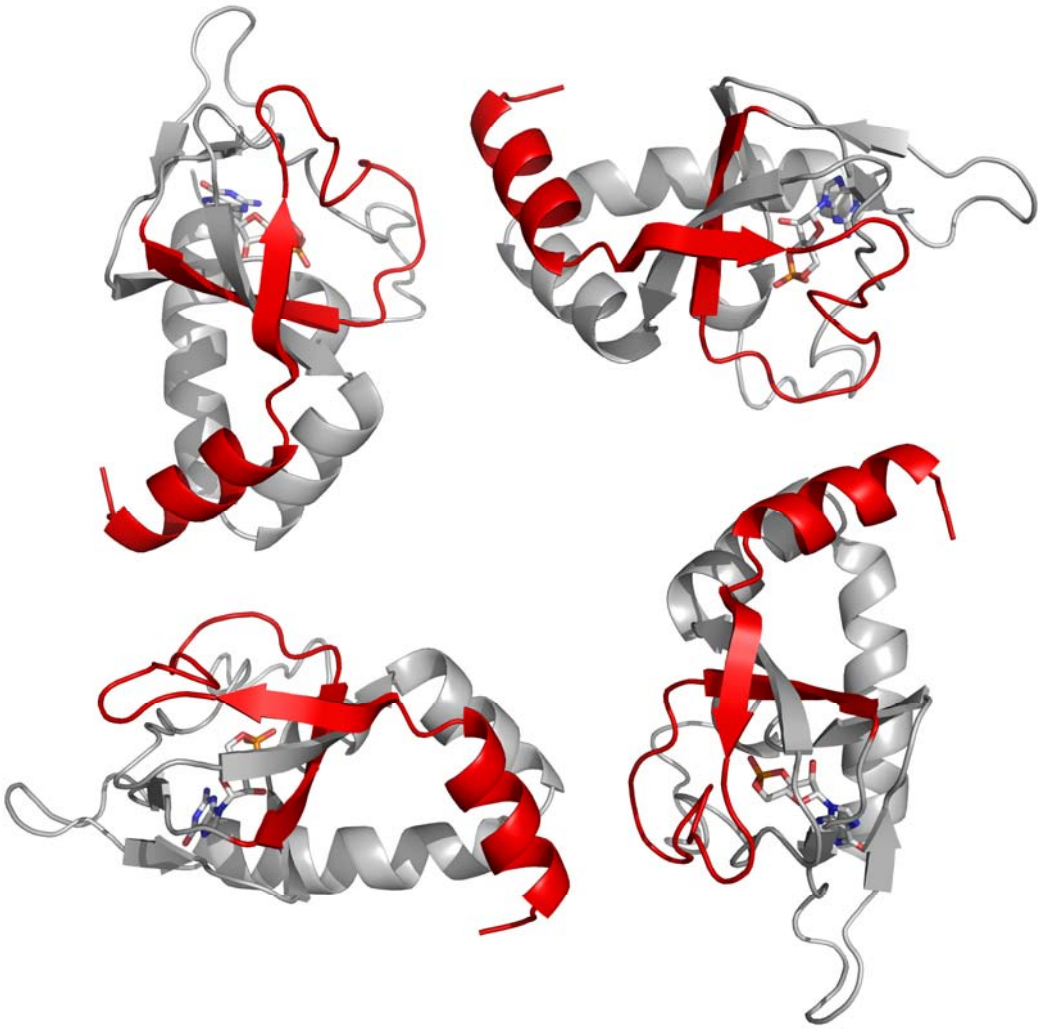

REFERENCE LIST

Altenhofen, W.J. LudwigE. EismannW. KrausW. BonigkU.B. Kaupp. 1991. Control of ligand specificity in cyclic nucleotide-gated channels from rod photoreceptors and olfactory epithelium. *Proc Natl Acad Sci U S A*. 88:9868-9872.

Arnold, K.L. BordoliJ. KoppT. Schwede. 2006. The SWISS-MODEL workspace: a web-based environment for protein structure homology modelling. *Bioinformatics*. 22:195-201.

Bezanilla, F. 2000. The voltage sensor in voltage-dependent ion channels. *Physiol Rev*. 80:555-592.

Biskup, C.J. KuschE. SchulzV. NacheF. SchwedeF. LehmannV. HagenK. Benndorf. 2007. Relating ligand binding to activation gating in CNGA2 channels. *Nature*. 446:440-443.

Bonigk, W.W. AltenhofenF. MullerA. DoseM. IllingR.S. MoldayU.B. Kaupp. 1993. Rod and cone photoreceptor cells express distinct genes for cGMP-gated channels. *Neuron*. 10:865-877.

Bradley, J.J. LiN. DavidsonH.A. LesterK. Zinn. 1994. Heteromeric olfactory cyclic nucleotide-gated channels: a subunit that confers increased sensitivity to cAMP. *Proc Natl Acad Sci U S A*. 91:8890-8894.

Bucossi, G.E. EismannF. SestiM. NizzariM. SeriU.B. KauppV. Torre. 1996. Time-dependent current decline in cyclic GMP-gated bovine channels caused by point mutations in the pore region expressed in Xenopus oocytes. *J Physiol*. 493 (Pt 2):409-418.

Chen, T.Y.K.W. Yau. 1994. Direct modulation by Ca(2+)-calmodulin of cyclic nucleotide-activated channel of rat olfactory receptor neurons. *Nature*. 368:545-548.

Clayton, G.M.W.R. SilvermanL. HeginbothamJ.H. Morais-Cabral. 2004. Structural basis of ligand activation in a cyclic nucleotide regulated potassium channel. *Cell*. 119:615-627.

Craven, K.B.W.N. Zagotta. 2006. CNG and HCN channels: two peas, one pod. *Annu Rev Physiol*. 68:375-401.

Dhallan, R.S.K.W. YauK.A. SchraderR.R. Reed. 1990. Primary structure and functional expression of a cyclic nucleotide-activated channel from olfactory neurons. *Nature*. 347:184-187.

Doyle, D.A.J. Morais CabralR.A. PfuetznerA. KuoJ.M. GulbisS.L. CohenB.T. ChaitR. MacKinnon. 1998. The structure of the potassium channel: molecular basis of K+ conduction and selectivity. *Science*. 280:69-77.

Eismann, E.F. MullerS.H. HeinemannU.B. Kaupp. 1994. A single negative charge within the pore region of a cGMP-gated channel controls rectification, Ca2+ blockage, and ionic selectivity. *Proc Natl Acad Sci U S A*. 91:1109-1113.

Fesenko, E.E.S.S. KolesnikovA.L. Lyubarsky. 1985. Induction by cyclic GMP of cationic conductance in plasma membrane of retinal rod outer segment. *Nature*. 313:310-313.

Gerstner, A.X. ZongF. HofmannM. Biel. 2000. Molecular cloning and functional characterization of a new modulatory cyclic nucleotide-gated channel subunit from mouse retina. *J Neurosci*. 20:1324-1332.

Gordon, S.E.W.N. Zagotta. 1995a. A histidine residue associated with the gate of the cyclic nucleotide-activated channels in rod photoreceptors. *Neuron*. 14:177-183.

Gordon, S.E.W.N. Zagotta. 1995b. Subunit interactions in coordination of Ni2+ in cyclic nucleotide-gated channels. *Proc Natl Acad Sci U S A*. 92:10222-10226.

Goulding, E.H.J. NgaiR.H. KramerS. ColicosR. AxelS.A. SiegelbaumA. Chess. 1992. Molecular cloning and single-channel properties of the cyclic nucleotide-gated channel from catfish olfactory neurons. *Neuron*. 8:45-58.

Goulding, E.H.G.R. TibbsD. LiuS.A. Siegelbaum. 1993. Role of H5 domain in determining pore diameter and ion permeation through cyclic nucleotide-gated channels. *Nature*. 364:61-64.

Goulding, E.H.G.R. TibbsS.A. Siegelbaum. 1994. Molecular mechanism of cyclic-nucleotide-gated channel activation. *Nature*. 372:369-374.

Guex, N.M.C. Peitsch. 1997. SWISS-MODEL and the Swiss-PdbViewer: an environment for comparative protein modeling. *Electrophoresis*. 18:2714-2723.

Hamill, O.P.A. MartyE. NeherB. SakmannF.J. Sigworth. 1981. Improved patch-clamp techniques for high-resolution current recording from cells and cell-free membrane patches. *Pflugers Arch*. 391:85-100.

Henn, D.K.A. BaumannU.B. Kaupp. 1995. Probing the transmembrane topology of cyclic nucleotide-gated ion channels with a gene fusion approach. *Proc Natl Acad Sci U S A*. 92:7425-7429.

Jan, L.Y.Y.N. Jan. 1992. Tracing the roots of ion channels. *Cell*. 69:715-718.

Jiang, Y.A. LeeJ. ChenV. RutaM. CadeneB.T. ChaitR. MacKinnon. 2003. X-ray structure of a voltage-dependent K+ channel. *Nature*. 423:33-41.

Kass, R.S. 2005. The channelopathies: novel insights into molecular and genetic mechanisms of human disease. *J Clin Invest*. 115:1986-1989.

Kaupp, U.B.T. NiidomeT. TanabeS. TeradaW. BonigkW. StuhmerN.J. CookK. KangawaH. MatsuoT. Hiroseet al. 1989. Primary structure and functional expression from complementary DNA of the rod photoreceptor cyclic GMP-gated channel. *Nature*. 342:762-766.

Kaupp, U.B.R. Seifert. 2002. Cyclic nucleotide-gated ion channels. *Physiol Rev*. 82:769-824.

Korschen, H.G.M. IllingR. SeifertF. SestiA. WilliamsS. GotzesC. ColvilleF. MullerA. DoseM. Goddeet al. 1995. A 240 kDa protein represents the complete beta subunit of the cyclic nucleotide-gated channel from rod photoreceptor. *Neuron*. 15:627-636.

Kumar, V.D.I.T. Weber. 1992. Molecular model of the cyclic GMP-binding domain of the cyclic GMP-gated ion channel. *Biochemistry*. 31:4643-4649.

Larkin, M.A.G. BlackshieldsN.P. BrownR. ChennaP.A. McGettiganH. McWilliamF. ValentinI.M. WallaceA. WilmR. LopezJ.D. ThompsonT.J. GibsonD.G. Higgins. 2007. Clustal W and Clustal X version 2.0. *Bioinformatics*. 23:2947-2948.

Liman, E.R.L.B. Buck. 1994. A second subunit of the olfactory cyclic nucleotide-gated channel confers high sensitivity to cAMP. *Neuron*. 13:611-621.

Liman, E.R.J. TytgatP. Hess. 1992. Subunit stoichiometry of a mammalian K+ channel determined by construction of multimeric cDNAs. *Neuron*. 9:861-871.

Liu, D.T.G.R. TibbsP. PaolettiS.A. Siegelbaum. 1998. Constraining ligand-binding site stoichiometry suggests that a cyclic nucleotide-gated channel is composed of two functional dimers. *Neuron*. 21:235-248.

Liu, D.T.G.R. TibbsS.A. Siegelbaum. 1996. Subunit stoichiometry of cyclic nucleotide-gated channels and effects of subunit order on channel function. *Neuron*. 16:983-990.

Long, S.B.E.B. CampbellR. Mackinnon. 2005. Crystal structure of a mammalian voltage-dependent Shaker family K+ channel. *Science*. 309:897-903.

Ludwig, J.T. MargalitE. EismannD. LancetU.B. Kaupp. 1990. Primary structure of cAMP-gated channel from bovine olfactory epithelium. *FEBS Lett*. 270:24-29.

Molokanova, E.B. TrivediA. SavchenkoR.H. Kramer. 1997. Modulation of rod photoreceptor cyclic nucleotide-gated channels by tyrosine phosphorylation. *J Neurosci*. 17:9068-9076.

Monod, J.J. WymanJ.P. Changeux. 1965. On the Nature of Allosteric Transitions: a Plausible Model. *J Mol Biol*. 12:88-118.

Nakamura, T.G.H. Gold. 1987. A cyclic nucleotide-gated conductance in olfactory receptor cilia. *Nature*. 325:442-444.

Neher, E.B. Sakmann. 1976. Single-channel currents recorded from membrane of denervated frog muscle fibres. *Nature*. 260:799-802.

Picones, A.J.I. Korenbrot. 1995. Spontaneous, ligand-independent activity of the cGMP-gated ion channels in cone photoreceptors of fish. *J Physiol*. 485 (Pt 3):699-714.

Rehmann, H.E. Arias-PalomoM.A. HaddersF. SchwedeO. LlorcaJ.L. Bos. 2008. Structure of Epac2 in complex with a cyclic AMP analogue and RAP1B. *Nature*. 455:124-127.

Root, M.J.R. MacKinnon. 1994. Two identical noninteracting sites in an ion channel revealed by proton transfer. *Science*. 265:1852-1856.

Ruiz, M.J.W. Karpen. 1999. Opening mechanism of a cyclic nucleotide-gated channel based on analysis of single channels locked in each liganded state. *J Gen Physiol*. 113:873-895.

Sambrook, J.a.D.W.R. 2001. Molecular cloning: a laboratory manual. Vol. Cold Spring Harbour Laboratory Press, Cold Spring Harbour, New York.

Shapiro, M.S.W.N. Zagotta. 2000. Structural basis for ligand selectivity of heteromeric olfactory cyclic nucleotide-gated channels. *Biophys J*. 78:2307-2320.

Shi, N.S. YeA. AlamL. ChenY. Jiang. 2006. Atomic structure of a Na+- and K+-conducting channel. *Nature*. 440:570-574.

Su, Y.W.R. DostmannF.W. HerbergK. DurickN.H. XuongL. Ten EyckS.S. TaylorK.I. Varughese. 1995. Regulatory subunit of protein kinase A: structure of deletion mutant with cAMP binding domains. *Science*. 269:807-813.

Tatusova, T.A.T.L. Madden. 1999. BLAST 2 Sequences, a new tool for comparing protein and nucleotide sequences. *FEMS Microbiol Lett*. 174:247-250.

Tibbs, G.R.E.H. GouldingS.A. Siegelbaum. 1997. Allosteric activation and tuning of ligand efficacy in cyclic-nucleotide-gated channels. *Nature*. 386:612-615.

Trudeau, M.C.W.N. Zagotta. 2003. Calcium/calmodulin modulation of olfactory and rod cyclic nucleotide-gated ion channels. *J Biol Chem*. 278:18705-18708.

Ulens, C.S.A. Siegelbaum. 2003. Regulation of hyperpolarization-activated HCN channels by cAMP through a gating switch in binding domain symmetry. *Neuron*. 40:959-970.

Varnum, M.D.K.D. BlackW.N. Zagotta. 1995. Molecular mechanism for ligand discrimination of cyclic nucleotide-gated channels. *Neuron*. 15:619-625.

Weber, I.T.T.A. Steitz. 1987. Structure of a complex of catabolite gene activator protein and cyclic AMP refined at 2.5 A resolution. *J Mol Biol*. 198:311-326.

Weyand, I.M. GoddeS. FringsJ. WeinerF. MullerW. AltenhofenH. HattU.B. Kaupp. 1994. Cloning and functional expression of a cyclic-nucleotide-gated channel from mammalian sperm. *Nature*. 368:859-863.

Yau, K.W.D.A. Baylor. 1989. Cyclic GMP-activated conductance of retinal photoreceptor cells. *Annu Rev Neurosci*. 12:289-327.

Young, E.C.N. Krougliak. 2004. Distinct structural determinants of efficacy and sensitivity in the ligand-binding domain of cyclic nucleotide-gated channels. *J Biol Chem*. 279:3553-3562.

Young, E.C.D.M. SciubbaS.A. Siegelbaum. 2001. Efficient coupling of ligand binding to channel opening by the binding domain of a modulatory (beta) subunit of the olfactory cyclic nucleotide-gated channel. *J Gen Physiol*. 118:523-546.

Zagotta, W.N.N.B. OlivierK.D. BlackE.C. YoungR. OlsonE. Gouaux. 2003. Structural basis for modulation and agonist specificity of HCN pacemaker channels. *Nature*. 425:200-205.

Zagotta, W.N.S.A. Siegelbaum. 1996. Structure and function of cyclic nucleotide-gated channels. *Annu Rev Neurosci*. 19:235-263.

Zhou, Y.J.H. Morais-CabralA. KaufmanR. MacKinnon. 2001. Chemistry of ion coordination and hydration revealed by a K+ channel-Fab complex at 2.0 A resolution. *Nature*. 414:43-48.

Zufall, F.S. FiresteinG.M. Shepherd. 1994. Cyclic nucleotide-gated ion channels and sensory transduction in olfactory receptor neurons. *Annu Rev Biophys Biomol Struct*. 23:577-607.